1978

Radio-Frequency Size Effect Measurements on the Fermi Surface of Rhenium.

Terrence L. Ruthruff
Louisiana State University and Agricultural & Mechanical College

RADIO FREQUENCY SIZE EFFECT MEASUREMENTS ON THE FERMI SURFACE OF RHENIUM

A Dissertation

Submitted to the Graduate Faculty of the
Louisiana State University and
Agricultural and Mechanical College
in partial fulfillment of the
requirements for the degree of
Doctor of Philosophy

in

The Department of Physics and Astronomy

by
Terrence L. Ruthruff
B.S., University of California, Los Angeles, 1971
M.S., Louisiana State University, 1973
May 1978

ACKNOWLEDGEMENTS

Foremost I wish to thank Dr. Roy G. Goodrich for suggesting the problem and providing guidance and assistance throughout the course of the experiment. Special thanks are also due to Drs. Claude G. Grenier and John C. Kimball for many informative discussions and to Dr. Peter B. Johnson whose vitality provided great incentive during a difficult phase of the experiment.

To Jacqueline Tamas who so willingly and carefully typed this manuscript and was so helpful with all the myriad details I express my deepest thanks. I also wish to thank the staff of the departmental machine and electronics shops for their competent aid and advice on various aspects of the experiment.

I wish to acknowledge the National Science Foundation for providing financial support for the experiment under grants DMR73-02427 and DMR76-81866. The financial assistance received from the Dr. Charles E. Coates Memorial Fund of the L.S.U. Foundation donated by George H. Coates for preparation of this manuscript is gratefully acknowledged.

TABLE OF CONTENTS

LIST OF TABLES

LIST OF FIGURES

LIST OF FIGURES (continued)

ABSTRACT

Radio frequency size effect measurements have been made to determine the dimensions of and the nature of electronic interactions on the Fermi surface of rhenium. The dimensional calipers were obtained from two thin single crystal samples with surface normals parallel to the [0001] and [11$\bar{2}$0] crystallographic axes. Through comparison with the relativistic augmented plane wave (with spin orbit coupling) band calculation of Mattheiss and de Haas-van Alphen and geometric resonance measurements these calipers were assigned to five different segments of the Fermi surface.

A very detailed model of the sixth band hole surface has been constructed from the calipers assigned to this piece. The seventh band hole surface is found to be cleft along the ΓALM plane. The intersection of the eighth band electron cylinder with the ΓALM plane has been determined and is found to agree well with the predictions of the band calculation. The present measurements indicate that no ninth band surface exists for rhenium and that measurements previously attributed to that surface arise from a void in the eighth band surface centered at Γ.

It has been found that the electron-electron interaction dominates the temperature dependence of the

electron scattering frequency at temperatures below 5 K. This result is consistent with other RFSE and resistance measurements in other transition metals in this temperature range. It is shown that the enhancement of the electron-electron interaction in transition metals is an intrinsic property of these materials and cannot be explained solely in terms of properties shared with non-transition metals.

CHAPTER I

INTRODUCTION

Several different experimental studies and an elaborate electronic energy band structure calculation have been made to determine the Fermi surface (FS) of rhenium. It is well established that this surface is made up of fifth, sixth, and seventh zone hole pieces and an eighth zone electron piece. The topology and perhaps even the existence of a ninth zone electron piece is still uncertain. The radio-frequency size-effect (RFSE) can be used to obtain the extremal dimensions of certain electronic orbits on these various segments of the FS. A careful analyses of RFSE data, relying on previous studies as a model, can yield detailed information on the contours of the FS unobtainable by other methods. Through such measurements some of the discrepancies between previous experiments and theory might be resolved.

The RFSE can also be a useful tool in determining the nature of electron scattering processes at low temperatures. In the past few years it has been determined that the electron-electron interaction is much stronger in the transition metals than in other metals of the periodic table. This conclusion has been reached through the observation of thermal and electrical transport properties of these metals at low temperatures. The RFSE may be

useful in developing an explanation for this enhanced electron-electron interaction since it can be used to examine the properties of particular groups of electrons rather than the properties of the bulk material.

The first part of this thesis continues with a review of the previous studies of rhenium and a section describing the RFSE and its use in determining FS calipers. The final section in this introduction describes how the nature and relative strengths of various electronic interactions can be deduced from the temperature dependence of the amplitude of the RFSE signal. Chapter II deals with techniques used in preparation of suitable RFSE samples of rhenium and Chapter III describes the experimental apparatus and detection systems used. In Chapter IV the FS caliper data is analyzed and compared with results from previous studies. The final chapter presents the results of amplitude temperature dependence measurements and their implications.

A. Rhenium

Rhenium is a silvery white metal with a density of 21.034 gm/cm^3 at 26 C. This high density is exceeded only by that of platinum, iridium, and osmium. It has a melting point of 3180 C which is exceeded only by that of tungsten and carbon. Atomic element number 75, rhenium is a Group VII A 5d transition metal with an atomic electronic configuration of Xe core plus $4f^{14}5d^{5}6s^{2}$. Rhenium

crystallizes in a hexagonal close packed structure with room temperature lattice parameters a = 2.760Å and c = 4.458Å.

In the past several years many methods have been employed in an effort to determine the topology and dimensions of the FS of rhenium. The first pulsed-field de Haas-van Alphen measurements of Thorsen and Berlincourt[1] showed that extremal orbits about various pieces of the FS had areas ranging from 0.0077 to 0.579Å^{-2}. Joseph and Thorsen[2] subsequently made torsion balance de Haas-van Alphen measurements. Most of their data could be attributed to orbits on two pieces of FS, a small ellipsoid and a somewhat larger dumbbell. The symmetries observed in the basal plane data and the apparent degeneracy between these pieces of surface led them to tentatively center them at the point L on the edge of the Brillouin zone with the degeneracy along the A-L line. Further high-field de Haas-van Alphen measurements by Thorsen, Joseph, and Valby[3] confirmed this earlier data and yielded other signals attributed to a ninth zone electron surface (torus) and a seventh zone hole surface (larger ellipsoid). These assignments as well as the assignment of the small ellipsoid as a fifth zone hole surface and the dumbbell as a sixth zone hole surface were made in accordance with the proposed model of Mattheiss.[4] Mattheiss' model is based on a

relativistic augmented-plane-wave with spin-orbit coupling band structure calculation. The results of this calculation also predict the existence of an eighth zone electron piece (cylinder) with a gap at the center of the zone. He showed that certain portions of the eighth and ninth zone pieces were very sensitive to the Fermi energy used in the calculations. An increase of 0.005 Ry from the chosen Fermi level of 0.825 Ry caused a dramatic change in an extension of the eighth zone electron sheet along the A-H line and a change in the topology of the ninth zone electron sheet from a set of disconnected balls to an undulating torus.

High-field magnetoresistance measurements by Reed, Fawcett, and Soden[5] and magnetoacoustic measurements by Jones and Rayne[6] and Testardi and Soden[7] yielded further information on the larger pieces of FS in rhenium. Some of these observed orbits arise from the eighth zone electron sheet and others travel over several pieces of surface by means of degeneracies along the A-L line and magnetic breakdown in this vicinity.

A number of details of the FS of rhenium are still unknown. The topology of the ninth zone electron surface is still uncertain. A portion of the data of Thorsen, Joseph, and Valby was analyzed as having come from an orbit about the inner circumference of the torus but no orbit was observed from the outer circumference nor around any cross section of such a torus. There are also some

disagreements between experiments concerning the detailed shapes of other pieces of the FS. The RFSE calipers could help determine these details and thus provide a suitable framework for more refined theoretical models.

B. The Radio Frequency Size Effect

A free electron moving perpendicular to the direction of an applied magnetic field travels in a circular trajectory. If the center of this trajectory is stationary (i.e., the electron has no velocity components parallel to the magnetic field) then the electron's momentum is perpendicular to the radius vector from this center to the electron at all times. The locus of momentum vectors corresponding to this circular trajectory will sweep out a circular orbit in momentum space. This situation is shown in Figure 1 where the electron moves in the x-y plane, the field is applied along the z-axis, and the momenta lie in the k_x - k_y plane, where $\vec{p} = \hbar\vec{k}$. Note that the trajectory and orbit are similar but that in the time frame, indicated a-b-c-d, the orbit is rotated from the trajectory by 90° about the magnetic field axis.

Studies of the electronic properties of metallic crystals require an interaction between the electrons of the crystal and some external probe such as an electric field. Such an interaction will generally alter the energy

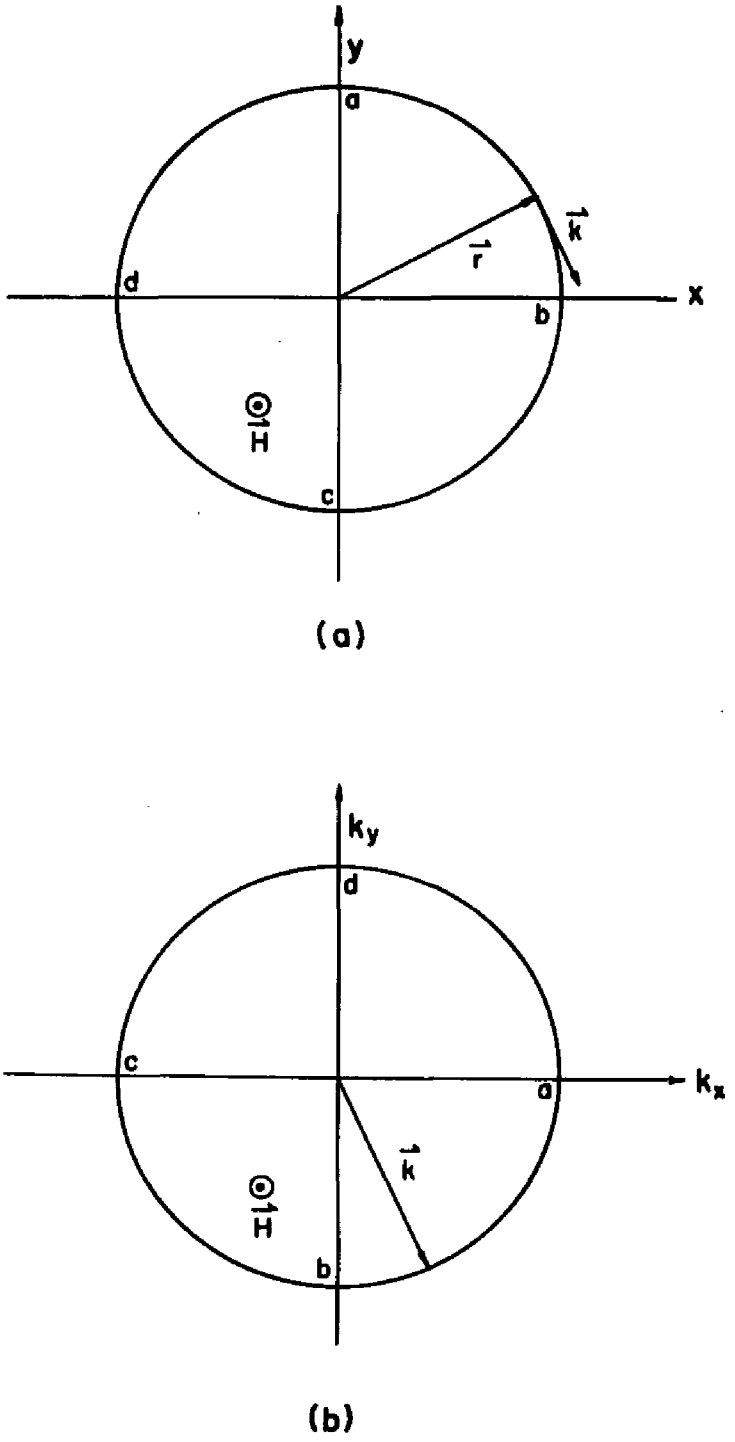

Fig. 1. a) Circular trajectory of a free electron in a magnetic field. b) The corresponding orbit in k-space.

of the electron in the crystal. Weak probing will yield information only on those electrons in energy levels within a band $k_B T$ about the Fermi level where k_B is Boltzmann's constant and T is the absolute temperature. Only this group of electrons can readily find alternate unoccupied energy states to enter as a result of the interaction with the probe. The electrons below this band are surrounded by filled states while negligibly few electrons are found above this band. In the RFSE the interactions of the metallic electrons with a radio frequency (r.f.) electric field are studied. This r.f. electric field can be considered a weak probe and only the properties of electrons on the FS will be observed.

When a magnetic field is applied to a metallic crystal the Lorentz force will cause the electrons to orbit as they would if free. Since this force is always perpendicular to the motion of the electron, it will not alter the energy of the electron. An electron initially on the FS (a surface of constant energy) will remain on this surface and orbit in a plane normal to the applied magnetic field. In real-space the electron's equation of motion can be written:

$$\vec{F} = \frac{d\vec{p}}{dt} = \hbar \frac{d\vec{k}}{dt} = \frac{e}{c}(\vec{v} \times \vec{H}) = \frac{e}{c}(\frac{d\vec{r}}{dt} \times \vec{H})$$

or

$$d\vec{k} = \frac{e}{\hbar c}(d\vec{r} \times \vec{H}) \qquad (1)$$

where $\vec{F}$ is the Lorentz force, $\vec{p}$ is the electron momentum, $\hbar$ is Planck's constant divided by 2π, $\vec{k}$ is the electron wavevector, e is the electron charge, c is the speed of light, $\vec{r}$ is the electron position, and $\vec{H}$ is the applied magnetic field. The projection of the electron trajectory on a plane normal to H will be a replica of the orbit but rotated 90° about the field direction as shown in Figure 2. Many possible electron orbits will not be centered at the origin of momentum-space. The corresponding trajectories will be helices with axes along the magnetic field direction. The relation between the dimensions of the orbit and trajectory is obtained through integration of Eq. (1):

$$K = \frac{e}{\hbar c} HD \qquad (2)$$

where D is the distance between any two points on the trajectory and K is the corresponding difference in momentum on the orbit.

For RFSE measurements samples are prepared in the form of thin slabs. An r.f. electric field ($\sim 10^7$ Hz) is applied parallel to the sample surface. At low temperatures the electron mean free path far exceeds the normal skin depth for these high purity samples. The r.f. electric field therefore penetrates to the anomalous skin depth δ which is on the order of 5 microns in the present

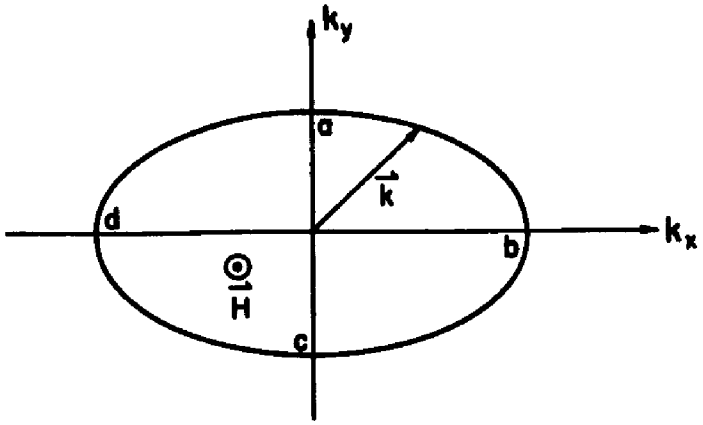

(a)

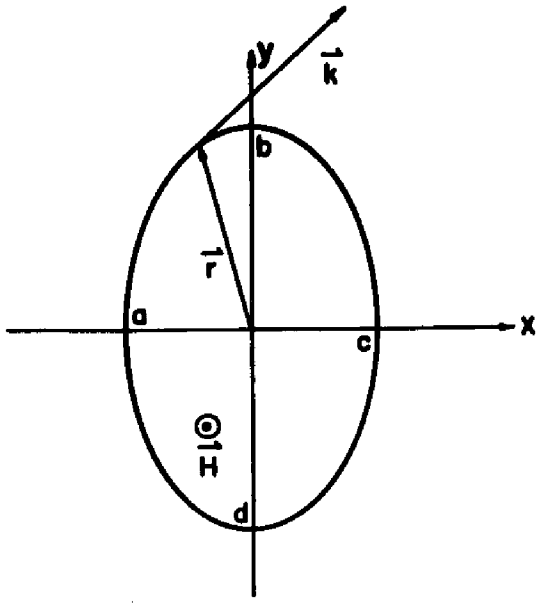

(b)

Fig. 2. a) An elliptical orbit in k-space. b) The corresponding electron trajectory in real space.

experiments. The electrons travel about their trajectories at the cyclotron frequency:

$$\Omega = \frac{eH}{m^*c} \quad . \tag{3}$$

which is of the order of 10^{10} Hz. During a pass through the skin layer the electrons see the r.f. electric field as being essentially static.

When an electronic trajectory is parallel to the sample surface within the skin layer the electron will be accelerated by the electric field there. At the bottom of such a trajectory this electron and others on the same trajectory will set up an r.f. current sheet deep within the sample. If this current sheet occurs within the skin layer of the other side of the sample the r.f. electric field will be radiated. That is the electrons on a sample spanning trajectory will transmit the r.f. electric field through the sample. Possible trajectories and their effects are shown in Figure 3.

For all but perhaps the lowest fields there will exist some orbit of diameter K such that D in Eq. (2) will equal the sample thickness, d. Consequently, some of the r.f. electric field will always be transmitted through the sample. The strength of the r.f. transmission will depend on the position of the orbit on the FS in the following way. The electrons participating in the transport process lie in

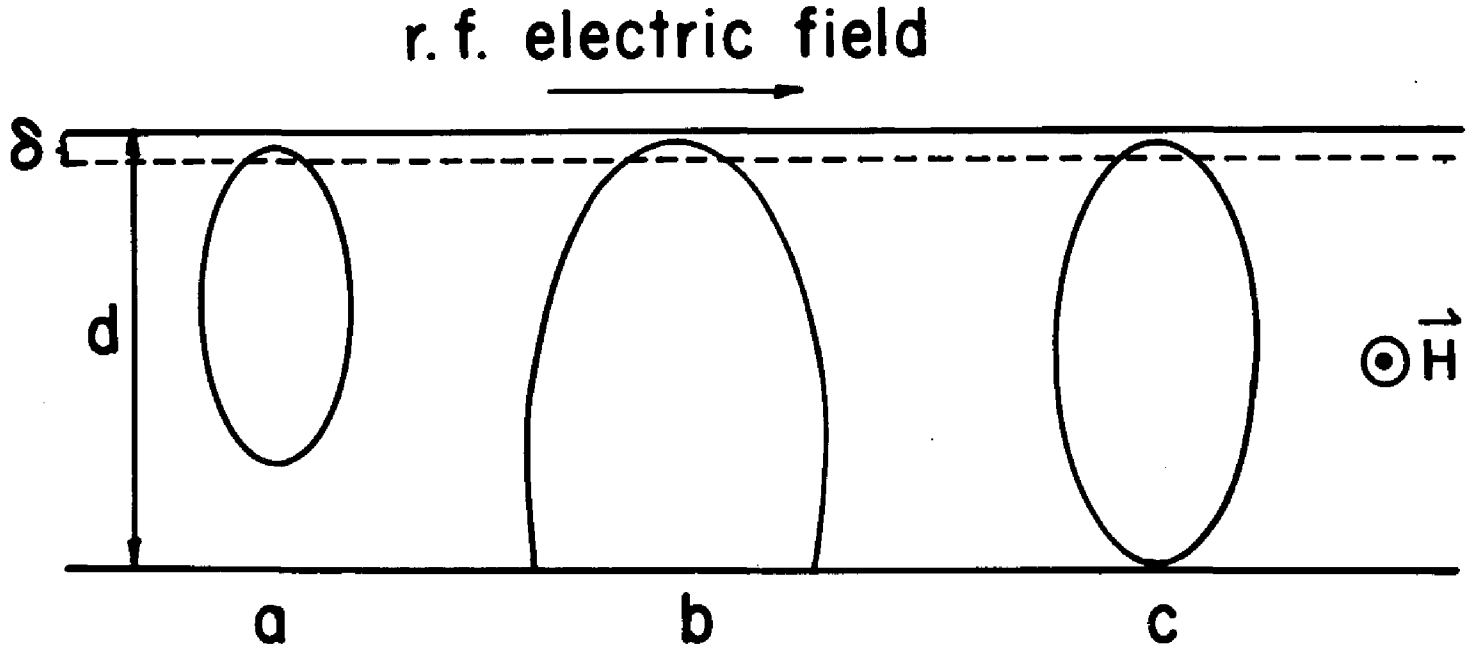

Fig. 3. Penetration of the r.f. field into the sample and possible electronic trajectories.

a band Δk of orbit diameters about K where $\frac{\Delta k}{K} \sim \frac{\delta}{d}$. In Figure 4 it can be seen that the number of electrons in this band and hence the strength of the transmitted r.f. depends on the location of this band on the FS. As the magnetic field is increased first the orbit a, then b, and finally c will give rise to the sample spanning trajectory. A gradual increase in the transmitted r.f. electric field will be detected by an antenna at the lower sample surface. As the magnetic field is increased further all trajectories arising from orbits on this segment of FS would be smaller than the sample thickness and a corresponding abrupt drop in the strength of the transmitted r.f. would be noted.

In practice these changes in r.f. level are small perturbations on a larger background level. A low frequency (to insure complete sample penetration) magnetic modulation field is added to the main magnetic field. Phase sensitive detection of the transmitted r.f. electric field strength then yields the first derivative of the sample transmission coefficient with respect to the magnetic field. This derivative is relatively insensitive to constant background or gradually varying r.f. levels. Signals occur due to abrupt changes in r.f. levels as when an orbit of maximum diameter, like orbit c in Figure 4, is responsible for the sample spanning trajectory.

In like manner signals are also seen from orbits of minimal diameter or any other time there are abrupt changes

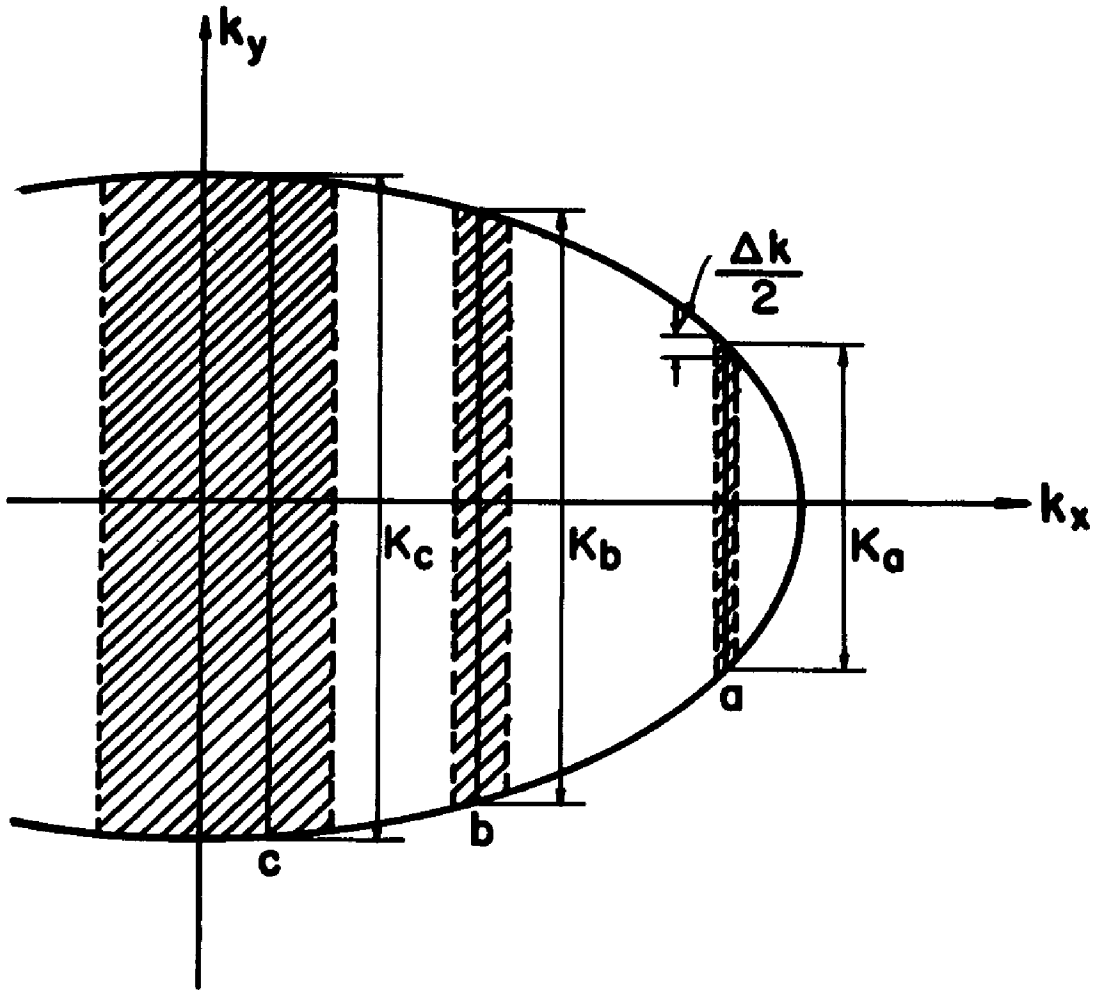

Fig. 4. The number of electrons participating in signal transport is proportional to the width of the band on the FS.

in the number of participating electrons. Signals can also occur when the sum of the diameters of the trajectories from any two or more extremal (maximal or minimal) orbits exactly spans the sample. In this case one trajectory creates an r.f. current sheet within the sample and a second one carries it to the other surface. The diameter of an orbit (caliper) giving rise to a signal can be determined through Eq. (2):

$$k_c = \frac{e}{\hbar c} H\, d \qquad (4)$$

where k_c is the extremal (usually) orbit diameter (caliper), H is the magnetic field at which the signal occurs, and d is again the sample thickness.

Radio frequency size effect measurements have been made using small transmitting and receiving antennas as described above.[8] These measurements were usually done to study the line shape of the RFSE signal. This complex line shape comes about because of the details of the penetration of the r.f. electric field into the sample. The transmitted field can be separated into quadrature components which yield information about the real and imaginary parts of the sample impedance.

A somewhat simpler and more widely used method is to place the sample in the tank coil of a marginal or limiting type oscillator. The changing numbers of electrons participating in sample spanning trajectories will cause changes

in the sample impedance which will be reflected in the coil impedance. Real impedance changes will result in a change of r.f. level in such an oscillator while imaginary impedance changes will result in a frequency shift. Each of these schemes has been used in the present experiment.

C. Electron Scattering in Metals

The probability of an electron contributing to an RFSE signal is inversely propotional to the probability that it will be scattered before completing an orbit. It is possible that an electron might complete several orbits before scattering. The RFSE signal amplitude can be written as a sum of the contributions from each pass:

$$A = A_o \sum_m \exp\left(-\frac{m\pi\bar{\nu}_{eff}}{\Omega}\right) \quad , \tag{5}$$

where m is the orbit number, $\bar{\nu}_{eff}$ is the total effective scattering frequency averaged over the orbit, and Ω is the electron cyclotron frequency. If the term $\pi\bar{\nu}_{eff}/\Omega >> 1$ so that there is a high probability that the electron will be scattered after completing just one orbit, then Eq. (5) can be simplified by considering only the first term of the summation:

$$A \approx A_o \exp\left(-\frac{\pi\bar{\nu}_{eff}}{\Omega}\right). \tag{6}$$

The total effective scattering frequency, ν_{eff}, is

made up of three components. If these scattering mechanisms can be considered to be statistically independent such that the total scattering probability is just the product of the individual probabilities then:

$$\bar{\nu}_{eff} = \bar{\nu}_I + \bar{\nu}_e + \bar{\nu}_P. \qquad (7)$$

The bar indicates a scattering frequency averaged over the electron orbit.

The component ν_I is the intrinsic temperature independent scattering frequency. It arises from any impurities, dislocations, or strains introduced during sample growth or preparation. This intrinsic scattering frequency is independent of the sample environment particularly the temperature. It is this component of the scattering frequency which is dominant over the other components at low temperatures.

The term ν_e is due to the electron-electron interaction. The likelihood that a scattering event will result from this interaction is proportional to the probability that a final state will be available to each of the interacting electrons. Such states occur in an energy region k_BT about the Fermi level and the electron-electron scattering frequency, ν_e, is thus proportional to T^2. The ν_P component arises from the electron-phonon interaction. Scattering of electrons within the shell k_BT about the Fermi level can be accomplished only by phonons with

energies $h\omega(\vec{q}) < k_B T$. The number of such phonons is proportional to T^2. The strength of the electron-phonon interaction depends on the square of the electron-phonon coupling constant which is proportional to T. The overall electron-phonon scattering frequency is thus proportional to T^3. Certain FS configurations can give other temperature dependencies for ν_p [9] but such situations do not occur in rhenium.

It is most convenient to write the last two terms of Eq. (7) as $\alpha' T^2 + \beta' T^3$. Substituting into Eq. (6) and taking the ℓn gives:

$$\ell nA \simeq \ell nA_o - \frac{\pi \bar{\nu}_I}{\Omega} - \frac{\alpha' \pi T^2}{\Omega} - \frac{\beta' \pi T^3}{\Omega}. \qquad (8)$$

The magnetic field at which a particular signal occurs and hence the electron cyclotron frequency depend on the sample thickness. The cyclotron frequency and the intrinsic scattering rate will be constants for a single signal in a given sample and Eq. (6) can finally be written in the form:

$$\ell nA \simeq C - \alpha T^2 - \beta T^3 \qquad (9)$$

where $C = \ell nA_o - \frac{\pi \bar{\nu}_I}{\Omega}$, $\alpha = \frac{\pi \bar{\nu}_e}{\Omega T^2}$, and $\beta = \frac{\pi \bar{\nu}_P}{\Omega T^3}$ are all constants. The determination of α and β from the temperature dependence of the RFSE signal amplitude yields information about the nature and relative strengths of the various scattering mechanisms.

CHAPTER II

SAMPLE PREPARATION

Samples for RFSE measurements are prepared in the form of thin metallic single crystal slabs. These slabs are cut from the bulk material with surface normals along specific crystallographic axes. This assures that the FS calipers obtained will lie or at least be projections on particular symmetry planes of the Brillouin zone. Most importantly the sample surfaces must be flat and parallel. Any irregularities in the sample thickness will allow an extremal orbit trajectory to span the sample over a range of magnetic field values. The resultant RFSE signal is field broadened and correspondingly diminished in amplitude.

Usable sample thicknesses are determined by the length of electron mean free paths. No RFSE signals can be observed unless a significant number of electrons can travel from one sample surface to the other without being scattered. At the low temperatures at which these measurements are made the dominant electron scattering arises from interactions with crystal impurities and dislocations (strain). Thus only high purity material is suitable for RFSE samples and the sample preparation must be carefully done to avoid introducing strain.

The sections of this chapter describe the steps taken in cutting, planing, and mechanically polishing rhenium

samples in preparation for RFSE measurements. Not all of these procedures were successful. The final optimum preparation scheme is outlined in the fourth section as well as the method used to determine the sample thicknesses. In the final section of this chapter a brief history of the samples prepared for this experiment is given.

A. Cutting

The first samples were prepared from a single crystal ingot of rhenium purchased from Materials Research Corporation (MRC). This material had a quoted purity of 99.996% and had been refined by six passes of an electron beam zone refiner. The ingot was in the form of an irregular rod one inch long and roughly 1/4" in diameter. Laue back reflection X-ray photographs showed that the [0001] crystallographic axis was approximately 15° from the cylinder axis.

The ingot was mounted with Duco cement and conductive silver paint on a two circle goniometer. It was then oriented using Laue photographs so that a slice could be cut normal to the [0001] axis. All cutting and planing was performed on a Servomet Spark Machine. Well aligned goniometer mounts in the spark cutter assured proper crystal alignment after orientation on the X-ray machine for each operation, cutting or planing.

Initial attempts at cutting the ingot were made using a taut tungsten wire as the spark cathode. At the lowest spark energy (range 7 ~ 25 mA. spark current) this wire eroded away after approximately fifteen minutes. Further attempts with this wire met with the same results and it was determined that this would not be a feasible technique. After two hours of cutting time the wires had penetrated only 0.025" into the side of the cylindrical ingot.

A piece was cut from a 0.010" thick sheet of tantalum and used as a cutting blade. This tool worked much better though it eroded away at about the same rate as the rhenium. It was very important to align the blade carefully in the vertical (cutting) direction. If the blade was slanted slightly, one face would be near one side of the cut and the groove would get wider as the blade descended. Not only would this be wasteful of the crystal material but it would also severely reduce the cutting rate. Even with the blade properly aligned the cutting edge became wedge shaped after several hours. The faces of the wedge presented large surfaces to the sides of the groove in the sample and the cutting rate was reduced.

A further difficulty was encountered when the cut had progressed about 3/4 of the way through the crystal. The thin slices being cut off were supported only by the uncut portion of the groove. As the cut progressed, the thin

slices would bend around this support point and close the groove on the blade. At this point cutting progress ceased altogether. The ingot was mounted on a thin aluminum finger of the goniometer. This finger allowed those portions of the blade on either side of the cut which were not eroded to pass clear of the goniometer. The crystal was mounted flush with the end of this finger so the finger would not interfere with the X-ray pictures. There was therefore no simple way to support the thin slab being cut. The solution was to very carefully remove the partially cut crystal from the goniometer, turn it over, and remount it using silver paint to fill the cut groove. The crystal was then re-oriented and the cut continued from the opposite side. The cause for this bending has not been determined but this phenomenon has been observed under similar circumstances with other relatively slowly cut metals. Total cutting time with the blade was about 50 hours.

Once a slice had been cut from the ingot it was etched in a boiling aqua regia solution (HCl and HNO_3, 3:1). During the etch a thin black film would slowly form on the freshly cut surface. After about ten minutes this film would peel off and no other reaction was observed. The composition of this film was not determined though two possibilities were considered. The film might have been a layer of alloying between the sample and cutting tool or

some rhenium-oxide layer grown during the cutting process. The oxide layer seems more reasonable in view of the fact that it was observed to form in the same fashion regardless of the cutting tool composition (tantulum, stainless steel, brass, copper). After all operations except cutting by tantalum wire (described later) the film was thick enough to prevent penetration of X-rays to the crystal. Laue back-reflection photographs could be made only after this film had been etched away.

No RFSE signals were observed in the first sample cut from the MRC ingot and it was felt that the purity was not sufficiently high. A second ingot was acquired on loan from L. Testardi of Bell Labs. This single crystal ingot was one grown by Soden, Brennert, and Buehler[10] and had a quoted residual resistance ratio ($R_{300K}/R_{4.2K}$) of 20,000. This was about a factor of 300 greater than we had measured for the MRC ingot. The ingot was in the form of a small cylinder about 1/4" long and 1/4" in diameter with [10$\bar{1}$0] crystallographic axis along the cylinder axis.

The use of the tantalum blade as a cutting tool was ruled out because of the small size of this ingot. The loss of material due to the blade thickness was more than could be afforded. A very simple moving wire attachment for the spark machine was built for cutting this ingot. This attachment consisted of two spools, a clock motor, and

two pulleys all mounted on a 3/32" thick sheet metal frame. The wire wound off the supply spool, across the two pulleys, and onto the 2 1/2" diameter take-up spool which was driven at one revolution per hour by the clock motor. The spark cutting occurred in a 2" gap cut out of the metal sheet between the pulleys. The wire was kept under tension by axial pressure from a spring on the support shaft of the supply spool. The cutting wire was 0.002" diameter tantalum purchased from California Fine Wire Co. and only very light tension was required to keep it taut and straight as it was advanced through the cutting space.

Best results were obtained when the pulley near the supply spool was locked down and the wire allowed to slide over it. This eliminated all sideways motion of the wire at this pulley. The sample and cutting attachment were set up so that the cutting occurred very close to the fixed pulley and the play in the other pulley, though slight, had very little effect. Spark cutting with this system proved to be very successful and the rod could be cut through in as little as fifteen hours. The wire was eroded nearly half way through on a single pass and could not be re-used.

B. Planing

The flat parallel-sided samples required for RFSE measurements were obtained by spark planing the cut slices.

The slices were mounted on the goniometer with silver paint and carefully oriented so that planing would occur normal to the desired crystal axis. This alignment was maintained when the goniometer was remounted in the spark machine. Planing was first done with the Servomet planing attachment and a six-inch brass disc. The brass disc was eroded away very quickly. The circumferential groove that was formed in the disc caused rounding-off of the edges of the sample before all the wire cutting marks had been removed from the center areas of the sample surface.

A stainless steel disc was made and fitted to the Servomet planer. Though this disc had been ground flat and the threads relieved to allow firm mating to planer, the surface of the disc moved up and down 0.001" at a 3-inch diameter as it rotated. The procedure for turning the disc suggested by Servomet was tried. This involved putting a carefully aligned block in place of the sample and reversing the spark polarity to make this block the tool and the planing disc the workpiece. This procedure might work for small irregularities in the planing disc but was not successful in removing this alignment problem. Apparently the planer had been too badly worn after 15 years of service.

A new planing attachment was designed and built and is shown in Figure 5. The principle objective of this design was to provide a true rotating, solidly mounted

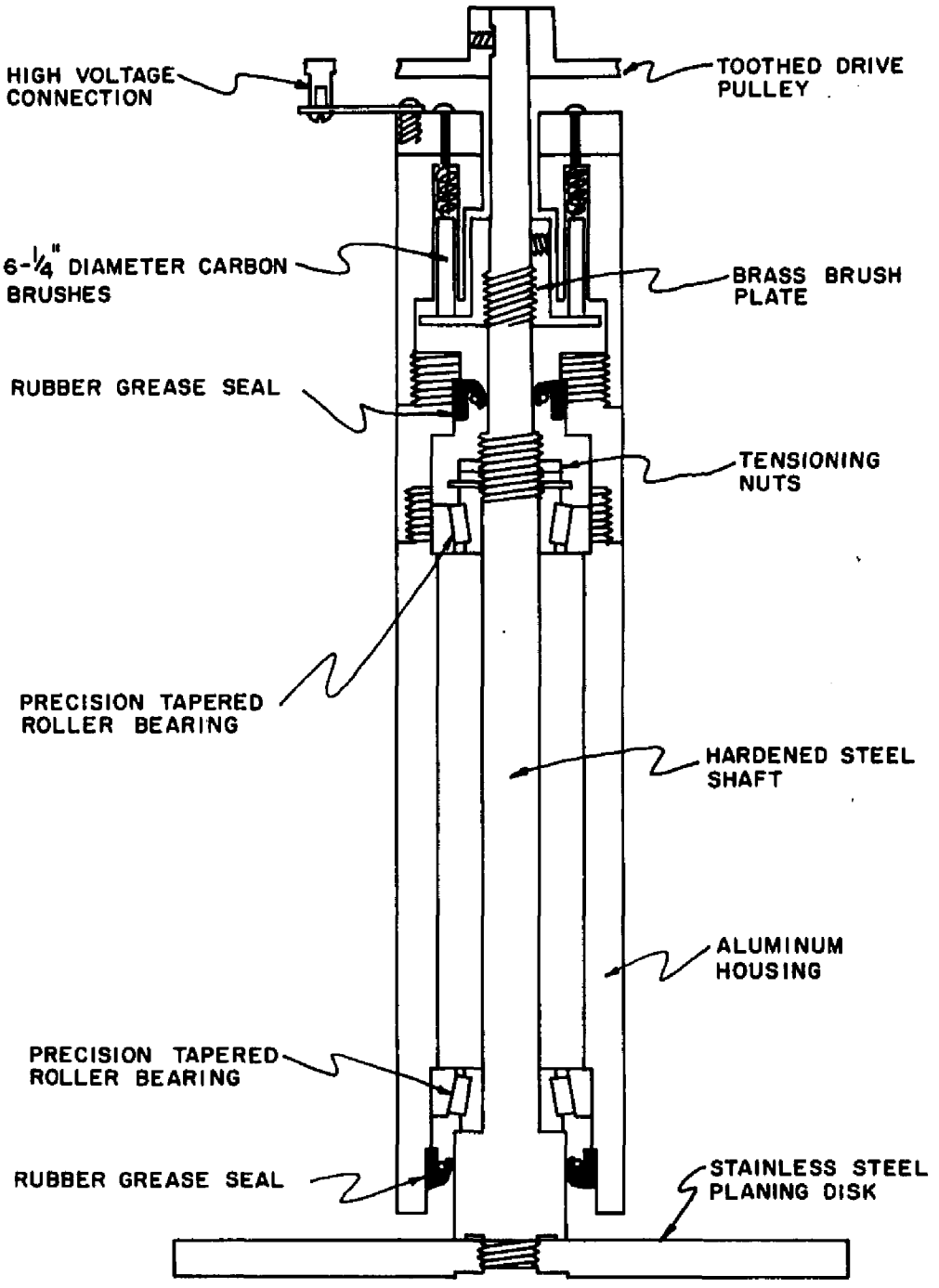

Fig. 5. Spark planing attachment.

shaft to support the planing disc. The planer would not only be used in the vertical position for ordinary planing but also horizontally to allow surfacing of the disc in position on the shaft. This objective was met through the use of a pair of high quality tapered roller bearings to support the steel shaft in the aluminum housing. During assembly the adjusting nuts were tightened until all detectable radial and axial play had been removed from the planer shaft. Some turning resistance resulted from this tightening but the drive motor easily overcame this. Rubber seals to the shaft above and below the bearings prevented contamination of the lubricating grease by entering dielectric fluid (kerosene or varsol). The brass disc and 1/4" diameter carbon brushes in the top of the planer insured good electrical contact to the shaft and disc and prevented the possibility of sparking through the bearings.

The planer was supported via a teflon collar in a magnesium (to reduce the overall weight) holder which also supported the drive motor. Disc rotation ($\sim$70 r.p.m.) was supplied by the motor through a toothed nylon belt. The teflon collar and nylon belt electrically insulated the planer from the frame of the spark machine. A second mount was made to hold the planer on the ways of a high precision lathe. The planer shaft was driven by a rubber tube attached to a drill motor and the disc was ground with an

electric grinder mounted on and traveling with the lathe cross guide. This surfacing was done very carefully and trueness of ±0.0002" at a 3 inch diameter was regularly achieved.

Using the new planer the previously cut and re-oriented slice was planed on one side until a flat surface was obtained. The steel planing disc wore very little during this operation and the sample edges were only slightly rounded. The sample was removed and the goniometer returned to its 0-0 position and remounted in the spark machine. The platform to which the sample was to be attached was then planed flat. Then, without changing the position of the planer other than to move it upward with the servo, the sample platform was cleaned with acetone and the planed side of the sample attached to the platform with silver conducting paint. The platform had previously been grooved to allow the paint to run out from under the sample. Care was taken to mate the planed surface of the sample closely to the freshly planed surface of the platform. This procedure assured that the second sample surface would be planed exactly parallel to the first despite any alignment errors which might exist between the X-ray and spark machine goniometer mounts. As long as the sample normals were within ±1/2° of being parallel to the desired crystallographic axis the necessity for parallel sides dominated the choice of planing procedure.

Once the initial planing had been completed on both sides a second planing was done at different radii on the disc or with a freshly surfaced disc to remove any rounding that may have occurred. This second planing required only short periods of time and the disc suffered no noticeable erosion. The freshly planed and etched sample surface was a dull whitish gray. This surface became darker as it acquired skin oils or other contaminants during handling. When viewed under a microscope the surface appeared to be very finely and uniformly pitted with the spacing between pit centers being 3 to 5 microns.

C. Polishing

No RFSE signals were observed in the first samples cut from the Bell Labs ingot and it was decided that this might be due to the irregular surface left after the spark planing. Though an optically finished surface might degrade the RFSE signal due to specular reflections of the electrons,[11] it was felt that some polishing might help. A No. 65-1506 AB Varimet Polisher/Grinder was used to mechanically polish these spark planed samples. This machine slid the sample radially across a 6" rotating disc. A Texmet cloth was mounted on the disc and silicon carbide and alumina powders ranging from 25 microns down to 1 micron suspended in water were used as polishing compounds. A separate disc and

cloth was maintained for each of the four different grits and the sample and holder were thoroughly cleaned whenever grit size was changed.

The sample holder consisted of a finely threaded brass disc and two case hardened steel rings with threads to mate to the disc. This holder had been accurately machined so that the axes of the disc and rings were well aligned and the surface of the disc was always parallel to that of the support ring. The sample was mounted to the disc with Duco cement and the support ring was adjusted to extend slightly beyond the sample surface as determined by a straight edge placed across a diameter of the ring. The other ring was screwed down tight against the support ring to lock it in position. Polishing was started and the sample was gradually lowered after ten-minute intervals until some effects of the polishing were noted. The disc and ring were scribed to make certain that this position did not change. An adapter was constructed to allow Laue back reflection photographs of the sample to be taken while it was still attached to the polishing mount.

Initial polishing with the 25-micron silicon carbide was very effective in removing the pitting left from the spark planing. The sample surface was visibly smoother and shinier though many small scratches were apparent. The X-ray photographs showed very little degradation due to the

initial polishing but continued polishing with this compound did cause surface strain. It is thought that the support ring may have polished away faster than the rhenium sample and caused the sample to be pressed too firmly against the cloth.

Similar results were obtained with the 15-micron alumina powder which was used next. This stage of polishing did leave the surface much shinier but rings characteristic of surface abrasion began to appear in the Laue photographs. Polishing with the finer compounds, 5-micron and 1-micron alumina powder, did not significantly improve the surface finish but did cause rounding of the sample edges and more abrasion as indicated by the Laue photographs.

The procedures above were developed using relatively thick (~0.5 mm) test samples cut from the MRC ingot. The strain damage to these samples was always confined to the surface and could be removed by spark planing to allow for further experiments with polishing. When these techniques were applied to the much thinner (~0.2 mm) samples cut from the Bell Labs ingot, different results were obtained. These samples were attached to the polishing mount with a very thin solution of Duco cement in acetone so that the glue could readily run out from under the sample to afford a good mating between the sample surface and the mount. As a

result most of the support occurred near the sample edges. For these thinner samples this did not provide a solid enough support against the forces of the polishing and the samples either separated from the mount entirely or partially and were strained before this situation was discovered. One sample each with normals parallel to the $[10\bar{1}0]$ and $[11\bar{2}0]$ axes cut from the Bell Labs crystal were destroyed in this way. Further attempts at producing usable samples by mechanical polishing were abandoned after this experience.

D. A Summary of Sample Preparation

The following steps were followed in preparation of the last three samples. These steps resulted in reliably strain-free, plane-parallel-faced rhenium samples suitable for RFSE measurements. First the ingot was mounted with Duco cement on a thin finger of a two-circle goniometer with care taken to keep the glue away from the actual cutting site. The ingot was then aligned for cutting using Laue back reflection X-ray photographs. Once satisfactory alignment had been attained extra glue was added to support the slice to be cut off and silver conductive paint was applied to insure good electrical connection between the sample and goniometer. The cut was then made using the 0.002" tantalum wire on the moving wire attachment for the spark cutter.

After cutting the slice was etched in an aqua regia ($HCl:HNO_3::3:1$) solution in a small beaker suspended in boiling water. The etch lasted approximately 15 minutes while a thin black film formed and peeled off of the freshly cut surface. The slice was then attached to a flat goniometer mount with silver paint and aligned for the first planing operation. This alignment was done very carefully as it determined the orientation of the final sample. The first side of the sample was planed flat and the sample was removed from the goniometer mount. The sample platform was planed to be parallel to the planer. The sample was attached to the platform with the freshly planed surfaces in firm contact and without disturbing the relationship between the planer and platform. The second sample surface was planed after the paint dried. Using the moving wire attachment and a coordinate slide on the spark cutter, the samples were trimmed to a parallelopiped shape.

The samples were then re-etched and weighed immediately before they became dirty. Typical mass was on the order of 50 mg and was determined to 0.01 mg. The perpendicular dimensions of the samples were then measured under a microscope. The eyepiece reticule was calibrated against a standard millimeter slide and the sample dimensions were reproducibly determined within a range of 0.2%. The sample volume determined from its mass and density of 21.034 gm/cm^3

was divided by the surface area to determine the average thickness. This method of thickness measurement was determined to be accurate to within 1%.

E. The Samples

In all, eight different rhenium samples were prepared. The first two (samples 1 and 2) with normals parallel to [0001] were cut from the MRC ingot. No signals were ever observed from these samples and they saw their greatest usefulness as test samples for the various preparation stages. Sample 1 was cut with the tantalum blade while sample 2 was cut with the moving wire attachment. Both samples were used to observe the effects of mechanical polishing. Sample 2 was also used to test a chemical polishing scheme by a procedure being used in the laboratory to thin and polish a gold RFSE sample. The aqua regia solution used to polish gold had no noticeable effect on the rhenium sample surface after 24 hours of polishing and this scheme was quickly abandoned.

Samples 3 and 4 were cut from the Bell Labs ingot with normals parallel to the $[10\bar{1}0]$ crystallographic axis. Sample 3 was strained during planing. It was discovered as a result of this accident that the planing disc could not be removed and remounted on the planer shaft with the required trueness. Each time the disc was removed it had

to be resurfaced after it was remounted and before it was used. Sample 4 was strained during a mechanical polishing stage. The loss of this sample was particularly painful since the cutting of a third sample of this orientation from the Bell Labs ingot would not have left sufficient material for samples of the other two orientations.

Samples 5 and 6 were cut from the Bell Labs ingot with normals parallel to the $[11\bar{2}0]$ crystallographic axis. Sample 5 was also strained during polishing and this stage of the preparation was subsequently deleted. The first signals were observed in sample 6 with an improved detection system (described in the next chapter) when it was 0.231 mm thick. The temperature dependence measurements were done on this sample and it was later thinned to 0.184 mm at which time the Fermi surface calipering was done.

Sample 7 was cut from the Bell Labs ingot with its normal parallel to the [0001] crystallographic axis. When it had been thinned to 0.190 mm no signals were observed. Further improvements of the detection circuitry finally yielded very weak signals from this sample. It was then thinned to 0.160 and 0.135 mm at which point the signals were strong enough to allow caliper determinations.

Sample 8 was cut from the MRC ingot with the surface normal parallel to the $[10\bar{1}0]$ axis. The lack of observable signals in the first samples cut from this ingot could not

be taken as an indication that no signals would be observed in samples of different orientations. The first samples cut from the MRC ingot had normals parallel to [0001] and it had been seen that in samples cut from the Bell Labs ingot the signals in a sample of this orientation were an order of magnitude weaker than those in a sample with the surfaces normal to [11$\bar{2}$0]. Furthermore the signal detection scheme had been greatly improved since any attempts had been made to observe signals from samples cut from the MRC ingot. Unfortunately there were still no signals to be found in this sample and the data analysis is based on signals seen only in samples 6 and 7.

CHAPTER III

THE EXPERIMENT

Rhenium was a very difficult material on which to make RFSE measurements. The relatively short electron mean free paths and the small size of the available single crystal ingots combined to make the signals weaker than any that have been observed in this laboratory before. As can be seen from the previous chapter a great deal of time and effort were spent before any RFSE signals were seen from rhenium samples. Much of this time was spent exploring the capabilities and advantages of alternative r.f. oscillator-detector systems. The results of these explorations are described in the second section of this chapter. First, the mechanical portions of the experiment are discussed. In the third section the signal conditioning and recording are described and the system used for the temperature dependence measurements is described in the final section. The experimental apparatus used for the cyclotron mass measurements required for the analysis of the temperature dependence data is presented in the appendix.

A. Mechanical Systems

All experiments were performed with the sample holder immersed in a liquid helium bath. The helium was contained in a conventional double glass dewar system. The outer

permanently evacuated dewar was filled with liquid nitrogen for initial precooling and heat shielding of the inner dewar. The vacuum jacket of the inner dewar was purged with air and pumped down several times before sealing prior to each run. This procedure prevented the accumulation in the jacket of any helium which might have seeped through the inner wall. Both dewars were silvered as further protection against radiative heat flow.

The helium dewar was supported by and sealed to a metal dewar head. This head also supported the sample holder and had ports for the pumping line and pressure gauge connections. The main helium pumping was done by a Kinney Model KD-110 high vacuum pump via a pumping control station. Besides allowing for straight through pumping this station provided for pressure (temperature) regulation both above and below the helium lambda point, 2.17K.

At temperatures above the lambda point the boiling of the liquid helium caused significant changes in the system pressure and regulation was best achieved by a flat rubber diaphragm type regulator. Such a regulator was sturdy enough to withstand these pressure changes but was capable of regulating the temperature of the bath only within a range of 0.1K. Below the lambda point helium is a superfluid and all boiling ceases. In this temperature range the system pressure changed only very gradually and

regulation could be achieved with a prophylactic tube regulator. This delicate regulation system worked as follows. All pumping was done through the prophylactic tube which was surrounded by a sealed housing. Initially this housing was vented to the helium dewar and the system was slowly pumped down. When the desired pressure was reached the regulator housing was sealed off. Any further pumping caused the pressure inside the tube to be lower than outside and it collapsed to constrict the pumping flow. An equilibrium pressure and pumping rate was rapidly reached. Although this system did not allow for accurate temperature adjustment it was capable of regulating the temperature within a range of 0.001K over a period of five minutes and 0.005K for as long as liquid helium remained in the dewar.

The tails of the dewars were necked down so they could be inserted in the bore of a six-inch air cooled electromagnet. The magnet could be rotated about the vertical axis making it possible to follow the calipers around the FS segments. The magnet was powered by an improved version of a 200-Watt field control supply designed and built in this lab.[12] This control allowed the field to be set anywhere in the range from -1000 to 1000 Gauss and swept from that value over a range of up to 1000G. The magnet control was designed to allow the low frequency field

modulation current to be superimposed on the main field current and up to 3 G peak to peak modulation fields could be attained this way. This proved insufficient for best detection of the RFSE signals from rhenium and a set of circular coils were wound on plexiglas frames and mounted on the magnet pole pieces. The reference output of the HR-8 phase sensitive detector was amplified and used to drive these coils to achieve a 6 G modulation. This was the largest modulation that could be used without over-modulating the signals.

B. Detection Systems

As mentioned in the introduction, several different detection systems were used. The first system had been used previously in this laboratory and utilized a high-level twin-triode marginal oscillator-detector described by Knight.[13] When used at high r.f. levels this oscillator worked in a limiting mode. In this mode a fixed amount of power was supplied to the L-C tank circuit of the oscillator. The level of oscillation was determined by the Q (quality factor) of this tank circuit. Real changes in the sample surface impedance due to the electron trajectories described earlier were reflected in the impedance of the coil which was wound around and closely coupled to the sample. An increase in the real impedance of the coil caused a reduction in the circuit Q and a reduction of the r.f.

level. The output stage of the oscillator rectified the r.f. signal and yielded an output proportional to the instantaneous r.f. level. A part of this output at the field modulation frequency was proportional to the derivative of the real part of the sample impedance with respect to the magnetic field, $\partial R/\partial H$.

The main body of the oscillator circuitry was mounted in an 1/8" thick brass box which was soldered directly to the top plate of the sample holder. The shielded vacuum tube projected from the side of this box to prevent overheating. The tube filament current was supplied by a storage battery and the bias was supplied by a high quality low noise power supply. The incoming power leads were shielded to help in the effort to keep any external electrical noise out of the circuit. The variable tuning capacitor shown in ref. 12 was replaced by a fixed value low-loss type to both raise the Q of the tank circuit and eliminate a potential source of noise. Any necessary tuning was accomplished by physically replacing this capacitor with one of a different value.

A 27-gauge copper wire was soldered to an insulated hermetic seal mounted in the top plate and led through teflon spacers down a 3/8" diameter thin wall stainless tube to the sample platform. The stainless tube, also soldered to the top plate, served as the outer conductor of

this coaxial line. A short piece of 27-gauge copper wire was silver soldered to the bottom of this tube for connection to the coil. The coils were wound with 40-gauge copper wire on steel forms. The forms were prepared from automotive type thickness gauges to be 50% thicker and 10-20% wider than the rectangular samples. These dimensions provided good sample-coil coupling and allowed the sample to be easily inserted without strain. Twenty-five to thirty turns were closely wound on the form and held in place with a very light coat of thinned Duco cement. Care was taken to see that the cement did not penetrate the coil and cause it to adhere to the form. The coil and form were then dipped in liquid nitrogen where the differences in thermal contraction caused the copper wire to stretch slightly. Upon warming to room temperature the coil could be carefully slipped off of the form.

Turns were removed from the coil until it was the same length as the sample. This left 20 to 25 turns and the coils had a free inductance of about 1 μh. The coils were mounted on the epoxy sample platform with Duco cement and the leads were stripped and soldered to the transmission line with Bi-Cd utectic solder. The use of standard Sn-Pb solder was avoided near the bottom of the sample holder. This solder becomes superconducting at liquid helium temperatures and could cause local distortions of the magnetic field.

Only faint hints of RFSE signals were observed in rhenium samples using this oscillator though several signals were seen from a cadmium test sample. This circuit was put aside for a time while the use of a MOSFET oscillator (to be discussed) was explored. A later rebuilding of this tube oscillator with changes made as a result of interim work improved its usefulness considerably. The changes included the use of low-loss silver mica capacitors throughout and careful component layout to avoid stray circuit capacitance. The first useful RFSE signals from rhenium were observed with this oscillator.

The second detection scheme that was tried involved the use of a MOSFET oscillator described by Slavin.[14] This oscillator was operated in the liquid helium bath with a buffer amplifier at the sample holder top plate, see Figure 6. The components for this MOSFET oscillator were chosen to have predictable characteristics and to withstand the stress of cooling to liquid helium temperatures. Such components included metal glaze resistors and silver mica and polystyrene and foil capacitors as well as the MOSFET. Again the sample was placed in the tank circuit coil of this oscillator.

Changes in the imaginary part of the sample-coil impedance due to RFSE signals resulted in a shift in the oscillator frequency. The magnetic field modulation caused

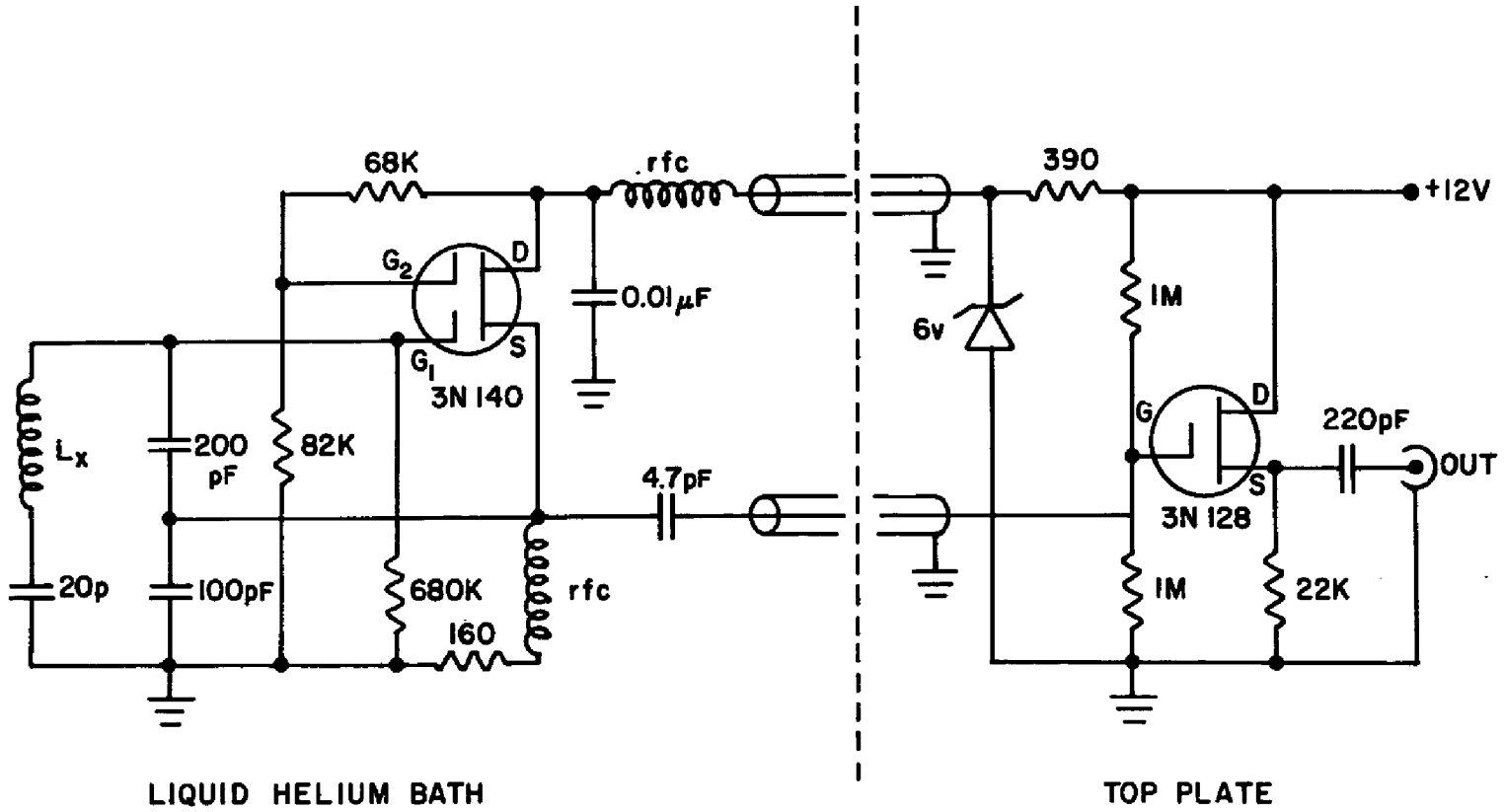

Fig. 6. MOSFET oscillator and buffer amplifier.

this shift to occur at the modulation frequency. The output of the oscillator was then a frequency modulated (FM) radio frequency carrier. The amplitude of the modulation was proportional to the first derivative of the imaginary part of the sample impedance with respect to the magnetic field, $\partial X/\partial H$. This frequency modulation can be converted to a voltage modulation suitable for phase sensitive detection by an FM discriminator.

Two such discriminators were used. The first was based on a design by Holman[15] as shown in Figure 7. In this circuit the oscillator signal and a stable reference signal were mixed by a dual gate FET. The sum signal was filtered out and the difference signal was amplified by several audio amplifier stages so that the final stage was saturated. The essentially square wave output of this final stage was used to trigger the pulses (IC 1). The width of the constant height pulses could be adjusted by the timing components associated with IC 1. These pulses were then integrated to yield an output level proportional to the pulse repetition rate which was in turn proportional to the difference frequency. The sensitivity of this discriminator could be adjusted over a wide range through selection of the reference frequency and the pulse width. The discriminator was insensitive to any changes in the amplitude of the r.f. carrier.

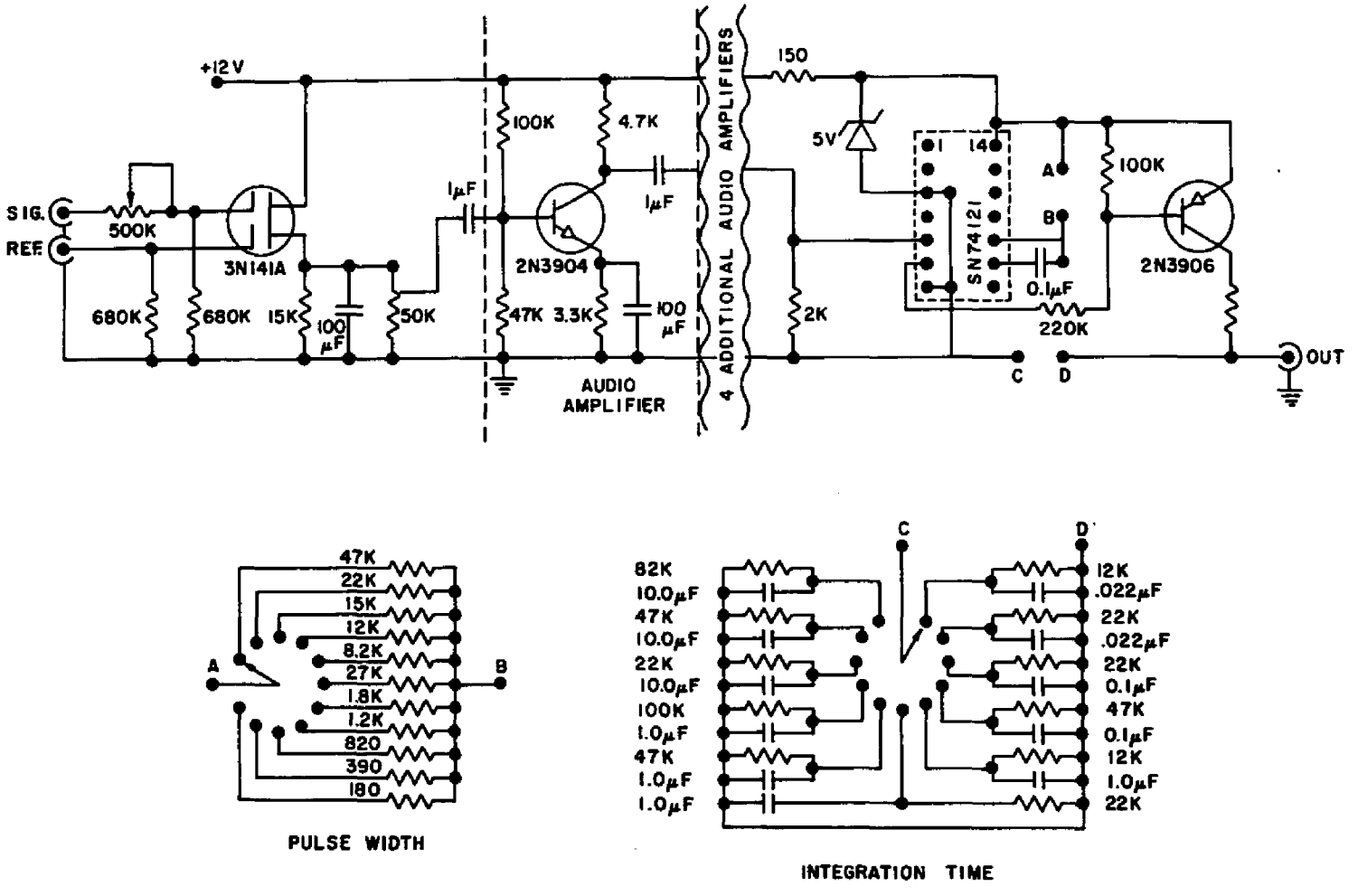

Fig. 7. FM discriminator.

The second discrimination scheme involved the use of a commercial FM tuner. The buffered oscillator output was coupled to the antenna terminals of the tuner which was then tuned to a harmonic of the oscillator frequency between 88 and 108 MHz. The output of the tuner was just a (sine wave) signal at the magnetic field modulation frequency with an amplitude proportional to the frequency excursions of the oscillator output. This signal was suitable for phase sensitive detection.

Signals were observed from the Cd test sample with each of these discriminators but the signal-to-noise ratio was not significantly improved over that of the tube oscillator. A large continuous drift in oscillator frequency with changing magnetic field led to problems in each case. At the tenth harmonic of the oscillator this drift was magnified ten times. Even with automatic frequency control (which normally helps a tuner track a signal shift due to local oscillator drifts) the tuner was unable to track the oscillator signal. The lab-built discriminator could be adjusted to handle the necessary range of oscillator frequencies but only at the expense of severely reduced sensitivity.

The MOSFET oscillator detection system was plagued by these 'dynamic range' problems and the difficulties of oscillator serviceability. It was nearly impossible to

make small changes in the oscillator circuitry and test them for improvements in sensitivity because the oscillator resided in the helium bath. Minor circuitry changes could easily be made in each of the other systems and be immediately evaluated while the sample remained at 4.2K and the oscillator at room temperature. Finally, uncertainties in the ability of the oscillator to withstand the repeated shock of cooling led to the abandonment of this detection scheme.

Efforts were turned toward a transistorized limiting oscillator described by Faulkner and Holman (FH).[16] A copy of this oscillator was built and installed on the sample holder. The initial results were discouraging because of high noise levels and a lack of sensitivity. At about this same period in time signals were finally seen with the rebuilt tube oscillator and it seemed best to stay with this for awhile. Over a period of time even the use of this tube oscillator became troublesome. The tubes would age unpredictably, the tube connections would become dirty and noisy, and large 60-cycle components appeared in the oscillator output despite all efforts to shield against the entry of external electrical noise. Meanwhile another member of the group was having fairly good results with the FH circuit.

This other FH circuit was borrowed and attached to the rhenium sample holder. The results were only nominal and efforts were made to determine the differences in the two systems. The main difference to be found was the size of the sample coils. The coils used for rhenium had only a tenth of the area of those used in other experiments. Such small coils were very lossy and contributed to a low L/C ratio both of which caused a reduction of the tank circuit Q. Not much could be done about the size of the coils since this was dictated by the dimensions of the samples. Therefore all efforts were concentrated toward reducing losses elsewhere in the circuit and preventing the entry of external electrical noise.

Several changes were made to the circuit to accomplish these goals. First a printed circuit board was carefully laid out to reduce all stray capacitance to a minimum particularly between the tank circuit and other parts of the oscillator. All capacitors used in the circuit were low loss silver mica types even though some compromises in value had to be made. Finally provisions were made to run the circuit off two nine-volt transistor radio batteries which resided in the brass box with the circuitry. These changes brought the performance of this circuit up to that of the tube oscillator.

The original FH circuit had been designed so that the level of the r.f. oscillation in the tank circuit could be adjusted through adjustment of the positive supply voltage. For certain magnetic resonance measurements low r.f. levels are necessary to avoid saturation of the signal. The amplitude of RFSE signals on the other hand were exactly proportional to the r.f. level. Further modifications were made to the circuit in the form of higher gain transistors and biasing resistors of lower value to give higher quiescent currents. The detector stage of the oscillator was also modified to give a balanced differential output. These changes resulted in an increase in r.f. level and RFSE signal-to-noise by an order of magnitude. The resulting circuit is shown in Figure 8.

The operation of each of the oscillators described was significantly different when the sample and coil were warm (300K) or cold (4.2K). With the transistor oscillator, for example, the r.f. level across the tank circuit was only 4 volts peak-to-peak with the sample in the coil at room temperature. On cooling to liquid nitrogen temperature (77K) this would increase to 6V. When the sample was cooled to 4.2K the r.f. level came up to 14V. This effect was not unexpected and can be attributed to the large residual resistance ratio ($R_{300}/R_{4.2}$ = 20,000) of the Re samples. At room temperature when the sample resistance is

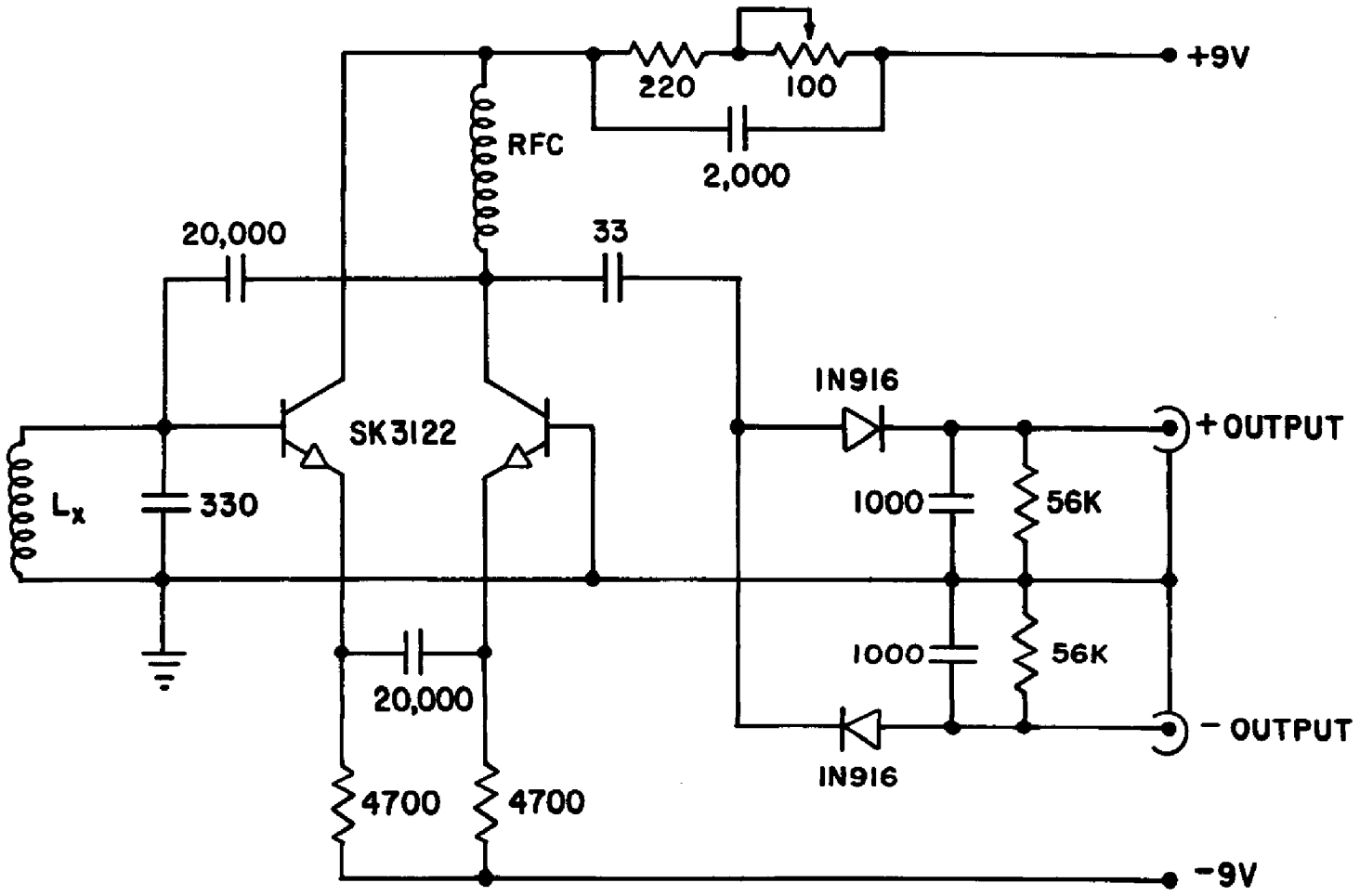

Fig. 8. Modified version of Faulkner and Holman limiting oscillator. Capacitance shown in pF.

high the r.f. electric field penetrates deeply into the sample. This penetration results in electrical losses and a lowering of the Q of the tank circuit. As the sample cools, its conductivity, σ, increases and the skin depth decreases as $\sigma^{-1/2}$. At 4.2K the normal skin depth is only $(20,000)^{-1/2} = 1/142$ of the room temperature value (note that if the skin depth is 5 microns at 4.2K then the r.f. field completely penetrates the sample at room temperature). With this much shallower penetration the losses in the sample are reduced. The Q of the tank circuit and thus the level of oscillation increases.

This effect was so dramatic that the tube oscillator would not operate while the sample was in the coil at room temperatures. Only when the sample was out of the coil or cooled to 4.2K could oscillation be sustained.

C. Recording RFSE Signals

The output voltage of the detecting oscillator or discriminator is the input voltage to a Princeton Applied Research model HR-8 lock-in amplifier. This input voltage consists of a large D.C. part, a small nearly sinusoidal part at the magnetic field modulation frequency (25-40 Hz.), and noise. The D.C. part is proportional to the mean r.f. level of the oscillator or the mean difference frequency of the discriminator and contains no useful information. The

noise consists mostly of 60 Hz. and harmonics thereof picked up in the system cabling and other low frequency (<100 Hz) components arising from mechanical vibration of the system. The useful RFSE information is contained in the amplitude variations of the sinusoidal part. Since most of the useful RFSE data was collected using the modified FH circuit, it is the details of this system which will be described.

The type A preamplifier of the HR-8 lock-in amplifier is equipped with two inputs (A and B) which can be operated in a differential mode (A-B). The output stage of the FH oscillator circuit was modified to take advantage of this differential input. As shown in Figure 8 the output stage of the oscillator (to the right of the 33 pf. capacitor) consists of a filtered full wave rectifier. The top and bottom of the r.f. envelope appear at the + and - outputs respectively. These outputs are connected by coaxial cables to the A and B inputs of the preamplifier. Any external electrical noise picked up in the oscillator circuitry, sample coil, or transmission line would be superimposed on the r.f. oscillations. Such noise would appear as an undulation of the constant amplitude r.f. envelope. This noise would appear with the same phase at the + and - outputs (A and B inputs) and would be eliminated by the differential (A-B) action of the preamplifier. Signal information appears as a modulation of the amplitude of the

envelope and that portion arriving at the - output is exactly 180° out of phase with the portion reaching the + output. In this case the differential action of the pre-amplifier yields the total variation of the envelope amplitude to be further amplified.

Any noise which enters the signal after the beginning of the rectification stage will not necessarily be common to both inputs of the preamp. Most noise of this type was picked up in the cabling between the oscillator and the preamp. A remote preamp adapter was used to allow placement of the preamp close to the oscillator so only short interconnecting cables were needed. A large reduction in pickup noise; mostly 60, 120, and 180 Hz; was realized when this arrangement was used.

After the information on the A and B inputs of the preamp has been differentially combined the resulting signal is amplified by broad band amplifiers in the preamp and the HR-8 mainframe. The signal is then amplified by a band pass amplifier tuned to the modulation frequency. Very little dispersion occurred at the modulation frequency (the r.f. carrier frequency was much greater than the modulation frequency) and the band pass amplifier could be operated at its highest Q (25) without loss of sensitivity. Noise components (from vibration) at frequencies very close to the modulation frequency which might have been amplified

by the band pass amplifier set at its normal Q of 10 were rejected at this higher Q value.

The signal is then mixed with a reference signal derived from the same source used to drive the field modulation. The phase of this reference signal is adjusted to match that of the information signal. The voltage of the D.C. difference signal resulting from this mixing is proportional to the amplitude of the sinusoidal variation of the amplitude of the r.f. envelope at the modulation frequency, i.e., the RFSE signal. Any higher frequency components of this mixed signal can be filtered by an adjustable low pass filter. The output of this filter is buffer amplified to provide the output used to drive the Y (vertical) axis of an X-Y recorder. The data was taken with the lock-in sensitivity adjusted in the range of 20-100 μV. At this sensitivity a 20 μV (100 μV) variation of the r.f. amplitude at the modulation frequency resulted in a 10 Volt D.C. output for an overall gain of $5(1) \times 10^5$.

A measure of the magnetic field was used to drive the X (horizontal) axis of the X-Y recorder. The original field control magnet control had been designed with an output proportional to the voltage induced on the feedback Hall probe mounted on the magnet pole face. This part of the circuit was replaced by an output proportional to the magnet current in the new version. Due to hysteresis

effects this new output was not representative of the magnetic field. A 0.25% linearity potentiometer was ganged in parallel with the sweep potentiometer of similar linearity and used to provide a voltage output proportional to the extent of the sweep. Tests showed this output to be a good measure of the field. The end points of the sweeps were calibrated before and after each experimental run against a Rawson-Lush Rotating-Coil Gaussmeter which had previously been calibrated against a NMR gaussmeter. The rotating coil was placed at the sample position in the dewar for the sweep calibration.

A drift in the magnet control circuitry between calibrations caused the calipers obtained on different runs to differ by as much as 5%. An F. W. Bell Model 600 Gaussmeter was purchased and the probe installed on one of the magnet pole faces. This gaussmeter was calibrated against the rotating coil gaussmeter to provide a 1 mV/Gauss output to a digital voltmeter. The range of the Bell gaussmeter was found to be stable to within 1/2% though the zero drifted by as much as 5 Gauss.

In nearly all RFSE measurements a signal near zero field has been observed which is typically one to two orders of magnitude larger than the RFSE signals. This zero field signal may be due to the low field magneto-resistance of the sample. It has also been observed that this signal

changes phase abruptly by 180° with respect to the modulation at zero field. This phase reversal was used during the experimental runs to adjust and monitor the zero of the Bell gaussmeter. The endpoints of the field sweeps were calibrated regularly by disconnecting the recorder input (which loaded the gaussmeter slightly) and reading the field value on the digital voltmeter.

The Bell gaussmeter responded to the modulation field as well as the main field. The modulation pickup caused some vibration along the recorder X axis. This vibration was removed by reducing the servo loop gain of the recorder without harmfully affecting the recorder response. The overall field calibration of the recordings was determined to be accurate to 1%. A schematic representation of this system is shown in Figure 9.

D. Temperature Dependence Measurements

Some measurements of the temperature dependence of the RFSE signal amplitudes were made with the apparatus described above. These measurements were made by regulating the temperature of the liquid helium bath using the regulators described in section A of this chapter. To make it possible to vary the sample temperature over a wider range, particularly above 4.2K, a different system was used.

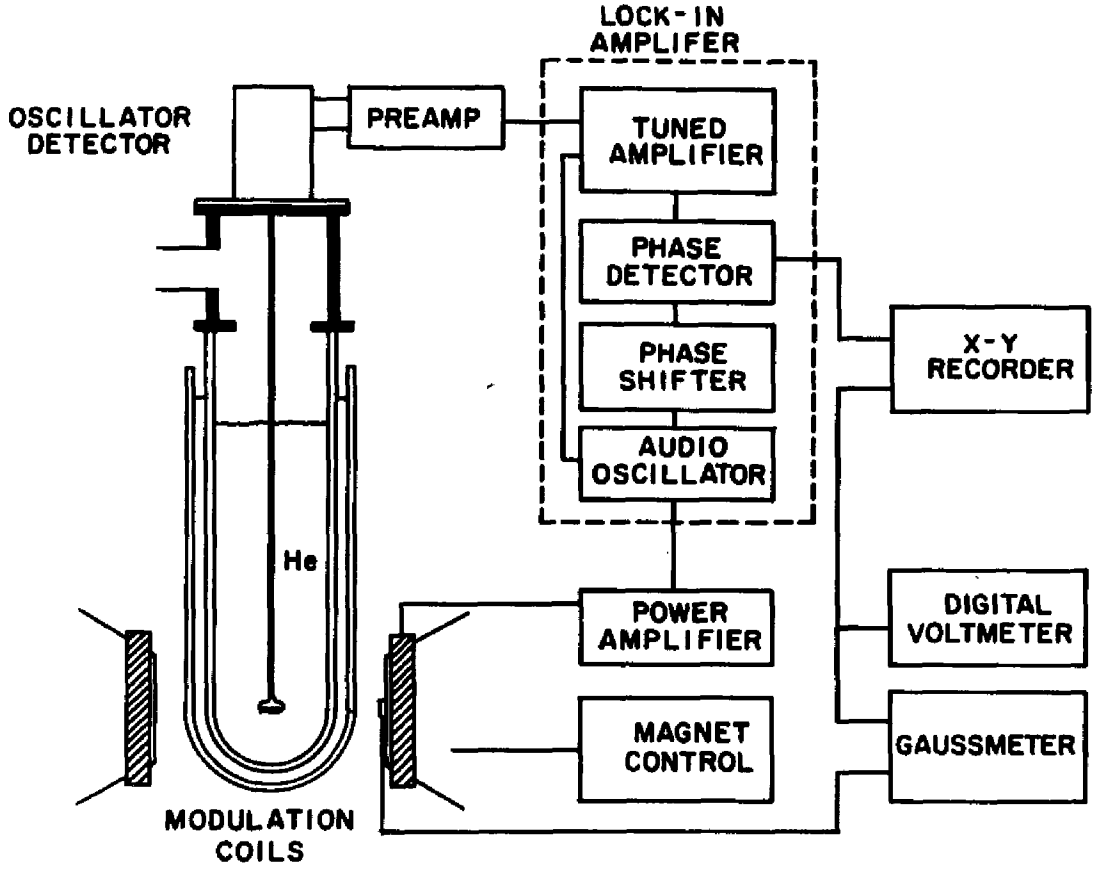

Fig. 9. RFSE system schematic.

In this second system the sample and coil were enclosed by two concentric thin-wall stainless steel cans. The outer can was immersed in the liquid helium bath, the space between the cans was evacuated to form an insulation space, and the inner can where the sample resided contained a small amount of helium exchange gas at a pressure of 2 mm of Hg. The helium bath was pumped down to 1.2K and regulated there by a prophylactic regulator. The sample and exchange gas could be heated above this temperature by current flowing in a heater wound on the inner can. The temperature of the sample was determined by measuring the resistance of a calibrated carbon resistor mounted near it.

The magnetic field was supplied by a Varian 12" electromagnet with 8"-diameter pole pieces controlled by a Fieldial Field Regulated Magnet Power Supply. The X axis of the chart recorder was driven by the output of the magnet controller supplied for this purpose. The remainder of this system was identical to the one used for calipering measurements.

CHAPTER IV

FERMI SURFACE CALIPERS

Three basic stages of analysis are involved in the determination of FS calipers from the recordings of RFSE signals. First the various angular series of signals must be identified, second a caliper point must be chosen for each series, and third each series must be assigned to a specific segment of the FS. At the end of the third stage the first two stages must be reexamined to assure that the whole analysis is self-consistent. Throughout the analysis a clear understanding of the crystal symmetries and the various orbit possibilities must be maintained.

For each sample the initial signals were recorded at 1° rotation intervals of the magnet in the plane of the sample. The caliper values obtained from these early recordings were of little quantitative value because of the magnetic field calibration drifts mentioned in the previous chapter. These recordings were however very useful in determining the angular extent and behavior of several series of signals which would have been much more difficult if larger angular intervals had been chosen. Some qualitative FS assignments were made on the basis of these early recordings.

It has been shown by Juras[17] and others that the line shape of an RFSE signal depends to some extent on the shape of the segment of FS supporting the signal orbit. A signal arising from an orbit about a spherical piece of FS can be distinguished from one arising from an orbit about a cylindrical piece. Although the line shapes predicted by such calculations were not used in the analysis per se, the line shape was a primary consideration in the initial assignment of individual signals to a series. Other initial considerations were that the amplitude of the signal and the value of the magnetic field at which the signal occurred would be relatively smoothly varying functions of the field orientation.

In most cases each series of signals was overlapped by one or more other series in some region of its angular extent. In a few cases a signal series was clearly separated from all others over only a very small angular region. Each series was carefully examined to locate a line shape which best typified the signals of that series. This signal was carefully traced and the points of maximum amplitude clearly marked. The caliper point was then chosen on this signal or another one of the series to be the beginning of the first major deviation of the signal from the background in accordance with the prediction of Juras.[17] It was in the determination of this caliper point

that the rewards for the circuitry modifications leading to improved signal-to-noise ratios were realized. Low pass filtering of 3 seconds time constant had been used in the lock-in to effectively remove noise from the early signals. This long time constant smeared the leading edge of the signal and made precise determination of the caliper point difficult. The final recordings made with the improved circuitry required only a 300 ms time constant and the caliper points of all but a few of the weaker signals were very clear.

Once a typical line shape and caliper had been chosen and drawn, each signal of the series was compared to this drawing and the caliper marked. Whenever a signal in the series was partially overlapped by another signal, those portions which were least affected by the overlap were used to determine the caliper point. For example, if a signal was overlapped slightly by one at a higher field, then the low field portions of the first signal would be used to determine the caliper point. The width of the signals in a series was watched carefully as the calipers were marked. This width might change as the curvature of the segment of FS over which the orbit passed varied as a function of the magnetic field orientation. Appropriate corrections to the caliper points were made when this was observed to happen.

Once all of the calipers had been marked and if the choice of signal series still seemed consistent, the caliper values were determined. Substitution of the values of e, $\hbar$, and c in Eq. (4) yields

$$k_c = 0.015194\ Hd \qquad (10)$$

where H is the magnetic field value in Gauss, d is the sample thickness in mm, and k_c is the orbit diameter in $\mathring{A}^{-1}$. The values of the magnetic field at the positions marked on the recordings were determined by extrapolation between the calibrated endpoints using a programmable calculator. These values and the appropriate sample thickness were then used to compute the caliper value by Eq. (10).

The computed caliper values were then plotted versus magnet angle. These plots were first examined to determine the relationship between the magnet angle and the crystal symmetry axis. This relationship was known approximately beforehand through knowledge of the orientations of the sample in the coil and the coil in the dewar. Centers of symmetry of the caliper versus angle plots corresponded to the magnetic field being parallel to one of the crystal symmetry axes. These plots were also examined for evidence of any signal series arising from combinations of orbits as described in Chapter I. Next, a polar plot was made of the caliper values versus magnetic field angle. It was in these

plots that the outlines of segments of FS really became visible. For signals arising from central orbits, those orbits whose plane contains a symmetry point of the Brillouin zone, the polar plot represented the intersection or projection of a segment of FS on the plane parallel to the sample surface.

The first Brillouin zone for the hexagonal close-packed crystal structure is shown in Figure 10. The labels commonly used in the literature to denote symmetry points in the zone and the directions of the [0001], [10$\bar{1}$0], and [11$\bar{2}$0] crystallographic axes are also shown. Note that all the information in the zone can be constructed from that contained in the small wedge with corners A L H K Γ M by symmetry. Five more equivalent [10$\bar{1}$0] axes from Γ to the center of the side faces of the hexagonal box and give more equivalent [11$\bar{2}$0] axes from Γ to the center of the side edges of the hexagonal box have not been shown. The dimensions of the lattice at 4.2K are: a = 2.758$\mathring{A}$ and c = 4.447$\mathring{A}$. Thus the Brillouin zone dimensions are computed to be: $\overline{\Gamma M}$ = 1.315$\mathring{A}^{-1}$, $\overline{\Gamma K}$ = 2($\overline{MK}$) = 1.519$\mathring{A}^{-1}$, and $\overline{\Gamma A}$ = 0.706$\mathring{A}^{-1}$.

The de Haas-van Alphen (dHvA) and geometric resonance measurements mentioned in Chapter I established the existence of four or perhaps five segments of the FS of rhenium. The intersections of these pieces with the faces of the A L H K Γ M wedge are shown in Figure 11. The outlines

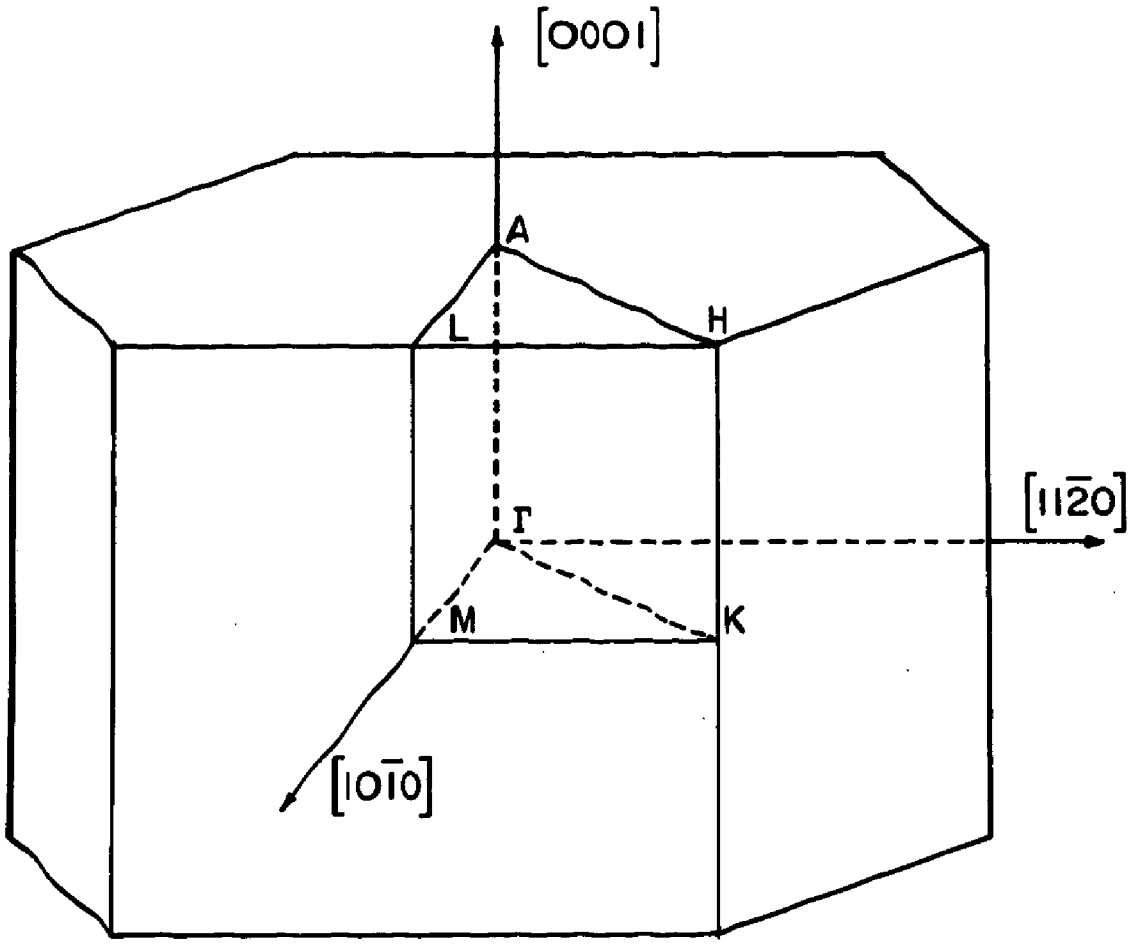

Fig. 10. Brillouin zone of hexagonal close packed lattice showing A L H K Γ M wedge.

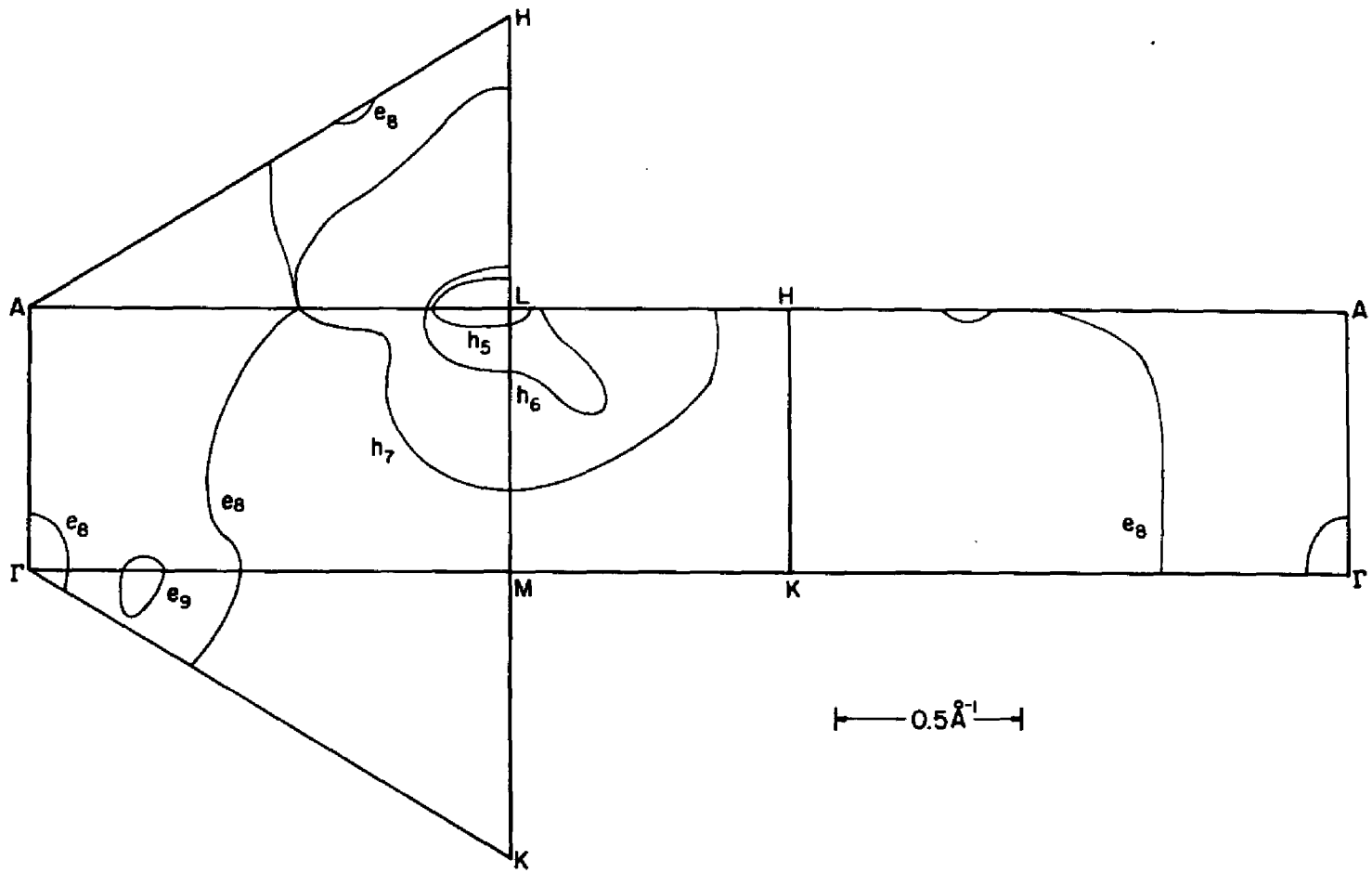

Fig. 11. Expanded A L H K Γ M wedge showing intersections of rhenium FS with symmetry planes after Mattheiss, E_F = 0.825 Ry.

shown are obtained from the APW calculation (including spin orbit coupling) of Mattheiss.[4] Three of these segments are centered at L on the edge of the Brillouin zone. The smallest of these is the fifth zone hole piece (h_5) which is a narrow ellipsoid (cigar) with its major axis along the A-L line. The sixth zone hole piece (h_6) (the dumbbell of Joseph and Thorsen[2]) surrounds the cigar and is degenerate with it along the A-L line. The seventh zone hole piece (h_7) surrounds both of these other pieces. The eighth zone electron sheet (e_8) is an undulating cylinder with its axis along the Γ-A line and open at both ends. This segment is degenerate with the seventh zone hole piece along the A-L line. A roughly spherical void in e_8 is centered at Γ. Finally, a ninth zone electron sheet (e_9) may exist as a set of balls situated on the Γ-M lines inside the eighth zone cylinder. Whether these balls are joined into an undulating torus or exist independently has not been previously conclusively determined.

In the following two sections the data obtained from samples with surface normals parallel to [0001] ($\hat{n}||[0001]$) and [11$\bar{2}$0] ($\hat{n}||[11\bar{2}0]$) are presented along with the results of the signal analysis. In the third section the caliper assignments are made and the resulting surfaces are compared with dHvA measurements and the predictions of the band calculation.

A. $\hat{n}\|[0001]$

All the calipers for this sample orientation can be obtained by rotating the magnetic field through the 30° range between the $[11\bar{2}0]$ and $[10\bar{1}0]$ axes in the plane of the sample. Those segments of FS centered at L on the edge of the Brillouin zone have 90° symmetry. The way in which this symmetry folds into 30° is illustrated in Figure 12. The ellipsoids shown are not intended to be representative of any particular segments of the FS but they do display the same symmetry properties as those segments centered at L. The orbits on three ellipsoids which are rotated 60° from each other yield the entire 90° of calipers in just 30° of magnetic field rotation. Note that three other ellipsoids not shown give the same calipers as those shown.

Typical RFSE signal recordings with $\bar{H}$ parallel to $[11\bar{2}0]$ (calipers along $[10\bar{1}0]$) and $[10\bar{1}0]$ (calipers along $[11\bar{2}0]$) are shown in Figure 13. These signals were assigned to six series labeled by Roman numerals I through VI. The caliper versus angle and polar plots are shown in Figures 14 and 15 respectively. The strongest signals seen in this sample orientation were nearly two orders of magnitude weaker than those seen in the sample with $\hat{n}\|[11\bar{2}0]$ when both were of comparable thickness ($\sim$0.18 mm). These signals were made somewhat stronger by thinning this sample

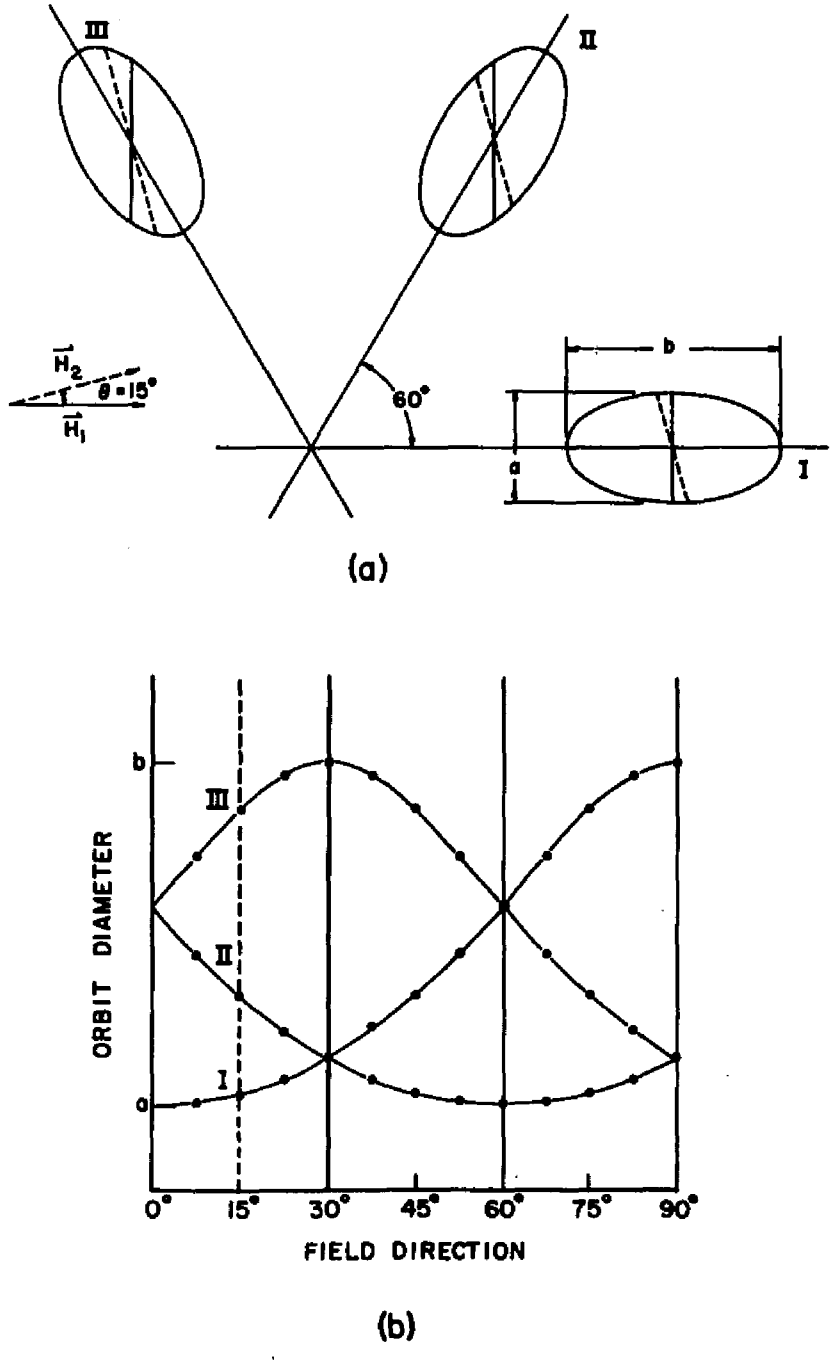

Fig. 12. Ellipsoids in basal plane. The entire 90° symmetry information is obtained by rotating the magnetic field through 30°.

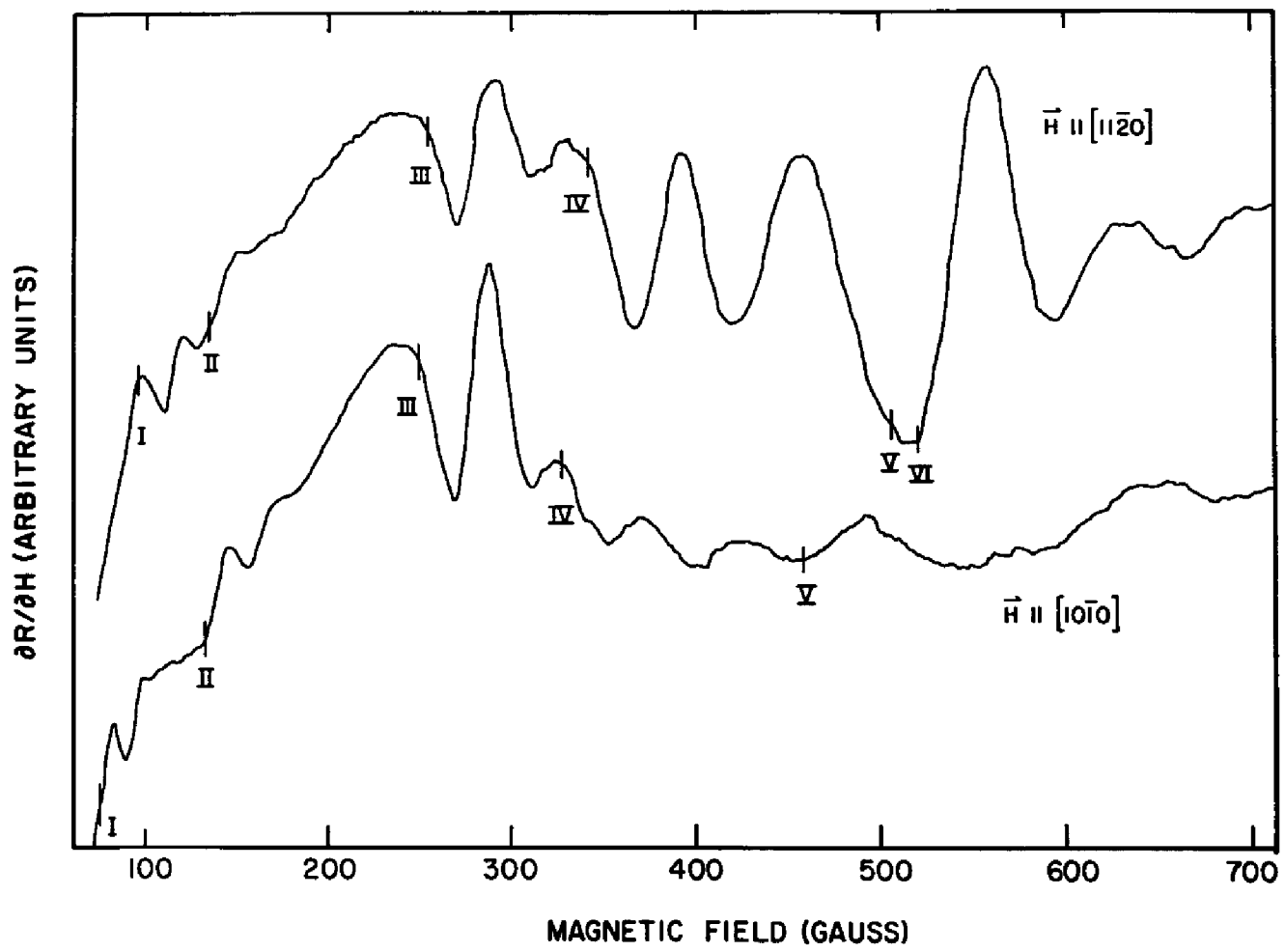

Fig. 13. Typical signal traces $\hat{n}\|[0001]$.

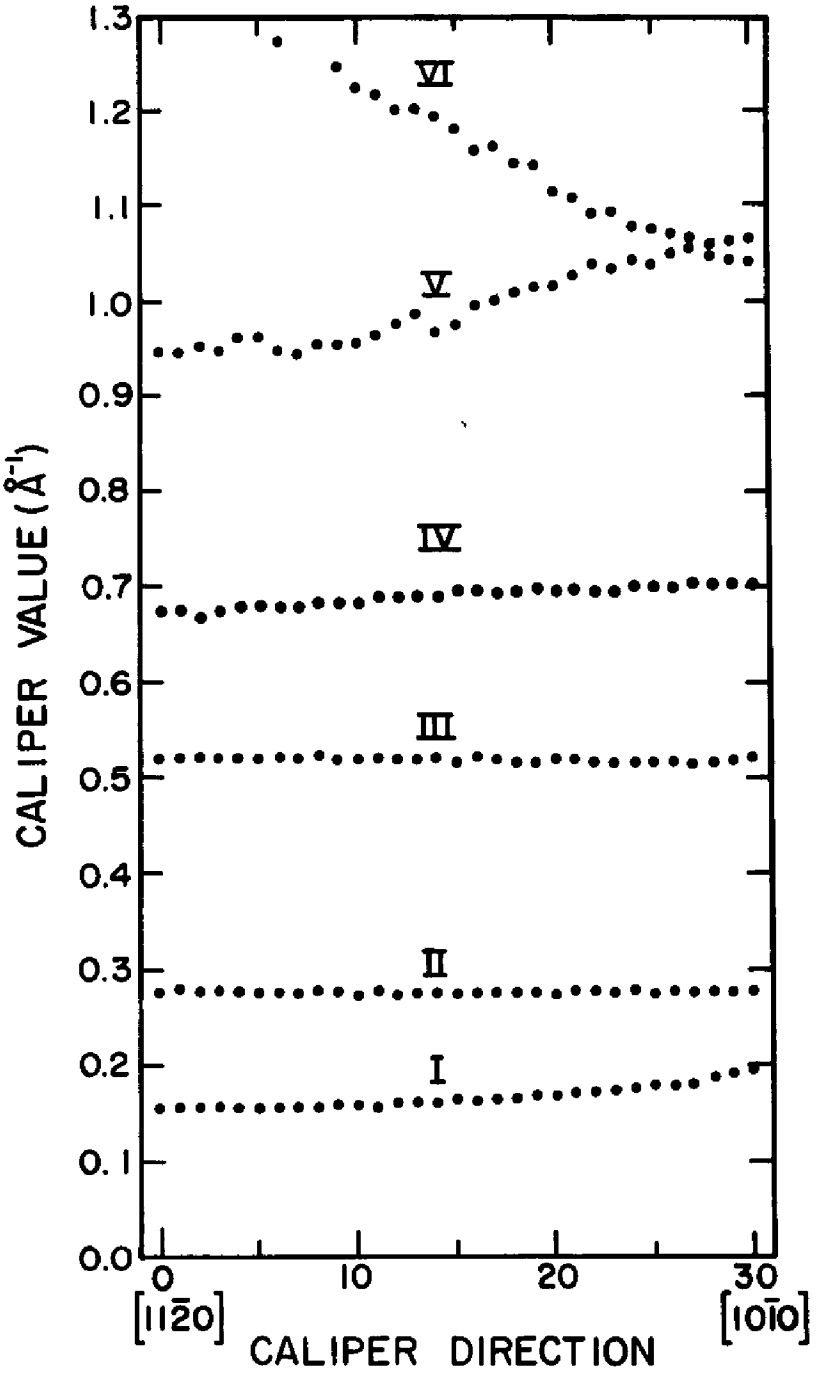

Fig. 14. Caliper vs. angle plot $\hat{n}$||[0001].

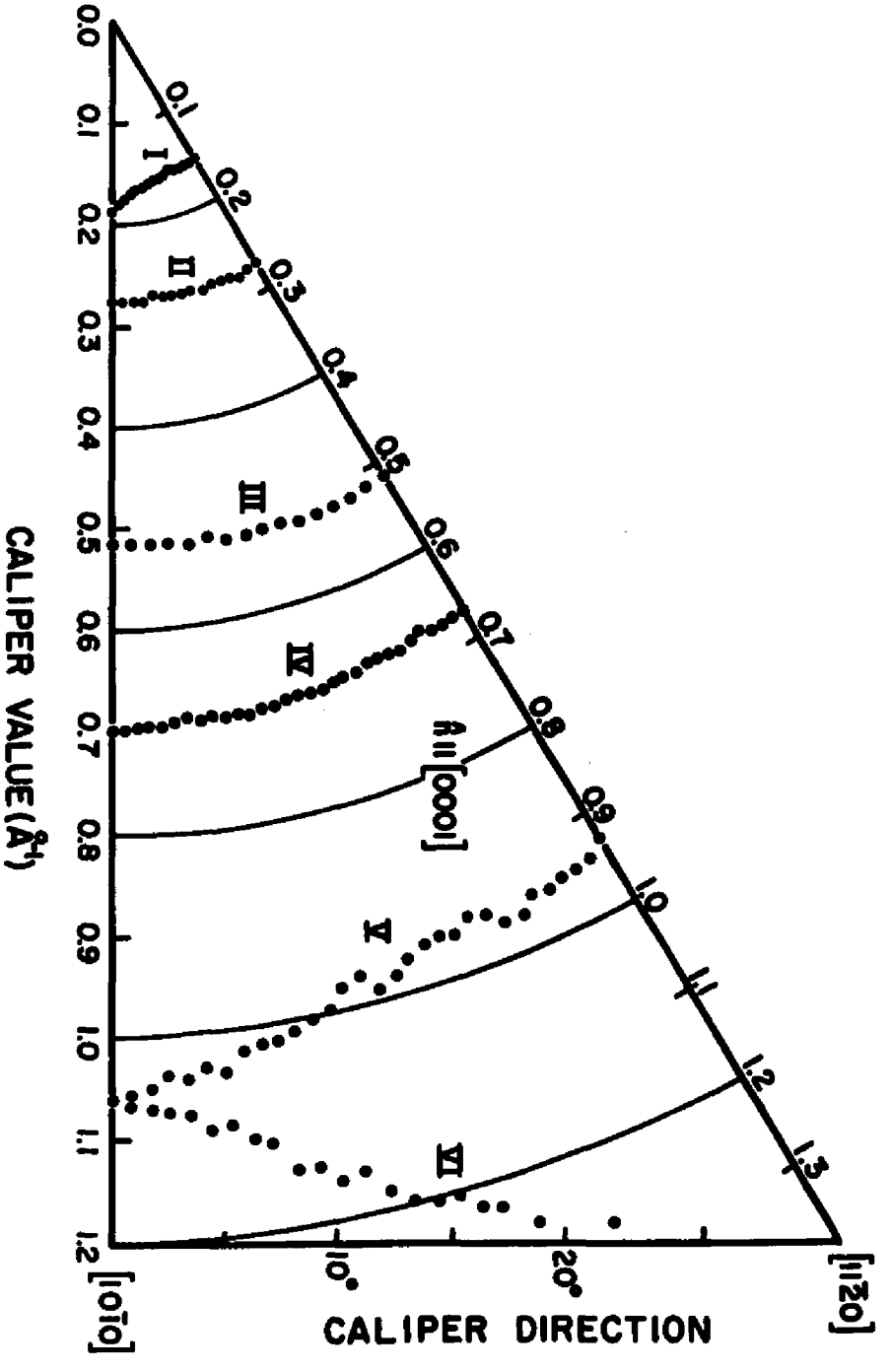

Fig. 15. Polar plot of calipers $\hat{n}$||[0001].

to 0.135 mm but still were only a quarter the amplitude of the others. Furthermore as the magnetic field was rotated from the $[11\bar{2}0]$ axis to the $[10\bar{1}0]$ axis the amplitudes of the signals in the top three series decreased by an order of magnitude while the amplitude of the signals of series III remained constant. This is thought to be due to the nature of the open orbits along e_8.

When the magnetic field is oriented along the $[11\bar{2}0]$ axis electrons travel along an open orbit on the surface of e_8 in the ΓALM plane, see Figure 11. The trajectory due to this orbit is roughly parallel to the sample surface. Electrons traveling along this trajectory can oscillate in and out of the sample skin layer as they travel along the surface. These electrons create an "artificial" increase in the sample conductivity and a commensurate decrease in the depth of penetration of the r.f. electric field. As the magnetic field is rotated toward the $[10\bar{1}0]$ axis the trajectory gets flatter until it reaches the shape depicted in Figure 11 as the intersection of e_8 with the ΓAHK plane. An electron traveling on this trajectory can remain in the skin layer for a relatively long period before it moves into the sample when it reaches the extension of e_8 along the A-H line. At low fields the trajectory along this extension might continue through the sample causing the electron to scatter at the far surface. As the field is

increased however the extent of this trajectory is decreased until it lies entirely within the sample. At this point the electrons can safely traverse the extension and return to the skin layer. It is the increase in surface conductivity and corresponding decrease in r.f. field penetration caused by these electrons that is believed to be responsible for the decrease of signal amplitudes above 300 Gauss in this sample. The caliper values obtained from this orientation are shown in Table I.

B. $\hat{n} \| [11\bar{2}0]$

The edges of the rectangular sample prepared for this orientation were parallel to the [0001] and [10$\bar{1}$0] crystallographic axes. In order to obtain good sample to coil coupling a coil was wound to have its axis parallel to the [10$\bar{1}$0] axis of the sample. When the magnetic field is aligned with the coil axis, it is perpendicular to the r.f. electric field and in the optimum configuration for detection of RFSE signals as described in Chapter I. As the magnetic field is rotated away from the coil axis the resulting electron trajectories are no longer parallel to the r.f. electric field at the sample surface. The RFSE signal amplitude therefore decreases as the cosine of the angle between the coil axis and the magnetic field. This decrease is hardly noticeable over the 30° range of magnet

Table I

$\hat{n}$||[0001] d = 0.135 mm

Caliper Direction	Series I	II	III	IV	V	VI
[10$\bar{1}$0]	.188	.277	.516	.700	1.047	1.060
1	.181	.277	.516	.700	1.056	1.067
2	.179	.277	.516	.698	1.049	1.071
3	.179	.275	.516	.698	1.038	1.076
4	.176	.277	.516	.698	1.042	1.078
5	.174	.275	.516	.693	1.033	1.094
6	.172	.277	.516	.693	1.038	1.091
7	.172	.277	.519	.695	1.020	1.107
8	.168	.273	.519	.693	1.015	1.114
9	.168	.275	.516	.695	1.013	1.143
10	.165	.275	.516	.693	1.009	1.145
11	.165	.275	.519	.691	1.000	1.163
12	.163	.275	.521	.693	..995	1.158
13	.165	.275	.516	.693	.975	1.181
14	.161	.1275	.521	.689	.968	1.194
15	.161	.273	.519	.689	.986	1.203
16	.161	.277	.519	.689	.975	1.203
17	.156	.273	.521	.689	.964	1.219
18	.159	.277	.519	.684	.955	1.226
19	.159	.277	.519	.682	.953	1.248
20	.156	.275	.523	.684	.955	
21	.156	.275	.521	.678	.944	
22	.156	.275	.521	.678	.948	1.275
23	.156	.275	.519	.678	.962	
24	.156	.277	.521	.680	.962	
25	.156	.277	.521	.673	.948	
26	.156	.279	.521	.669	.953	
27	.156	.277	.521	.675	.946	
28	.156	.275	.519	.675	.946	
29	.156	.279	.519	.673	.944	
[10$\bar{2}$0]	.156	.275	.519	.673	.930	

rotation used in the measurements in the previous section but becomes quite significant when the magnetic field has been rotated 45° from the coil axis.

In this orientation it is necessary to rotate the magnet through a range of 90° between the [0001] and [10$\bar{1}$0] axes. In order to acquire signals over this range a second coil was wound with its axis parallel to the [0001] axis of the sample. The RFSE signals were recorded with the magnetic field orientation rotated over a 55° range from the axis of each coil on separate runs. The data from both runs supplied the 90° symmetry information plus a 20° overlap region where the two sets of signals could be compared. The line shapes of these signals differed because of the different relative orientation of the r.f. electric field to the electron trajectories. The calipers obtained from these signals did however agree quite well in the overlap region.

Typical data traces taken with $\bar{H}$ oriented along [0001], 30° and 60° from [0001], and along [10$\bar{1}$0] are shown in Figure 16. The caliper values obtained are plotted versus angle in Figure 17 and a polar plot appears in Figure 18. The signals observed in this orientation have been arranged into nineteen series labeled by Roman numerals VII through XXV. The caliper values of each of these series are shown in Table II.

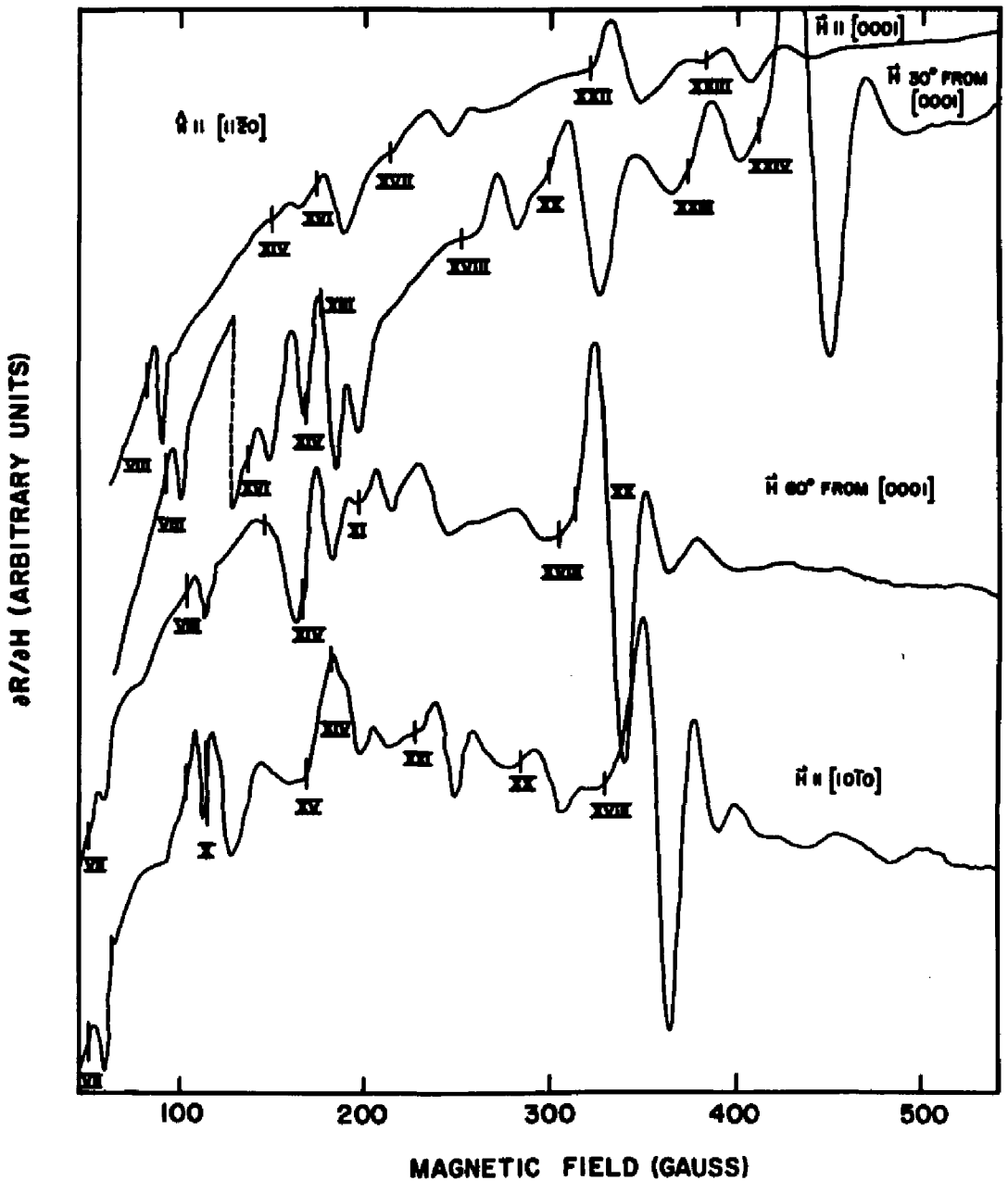

Fig. 16. Typical signal traces $\hat{n} \| [11\bar{2}0]$.

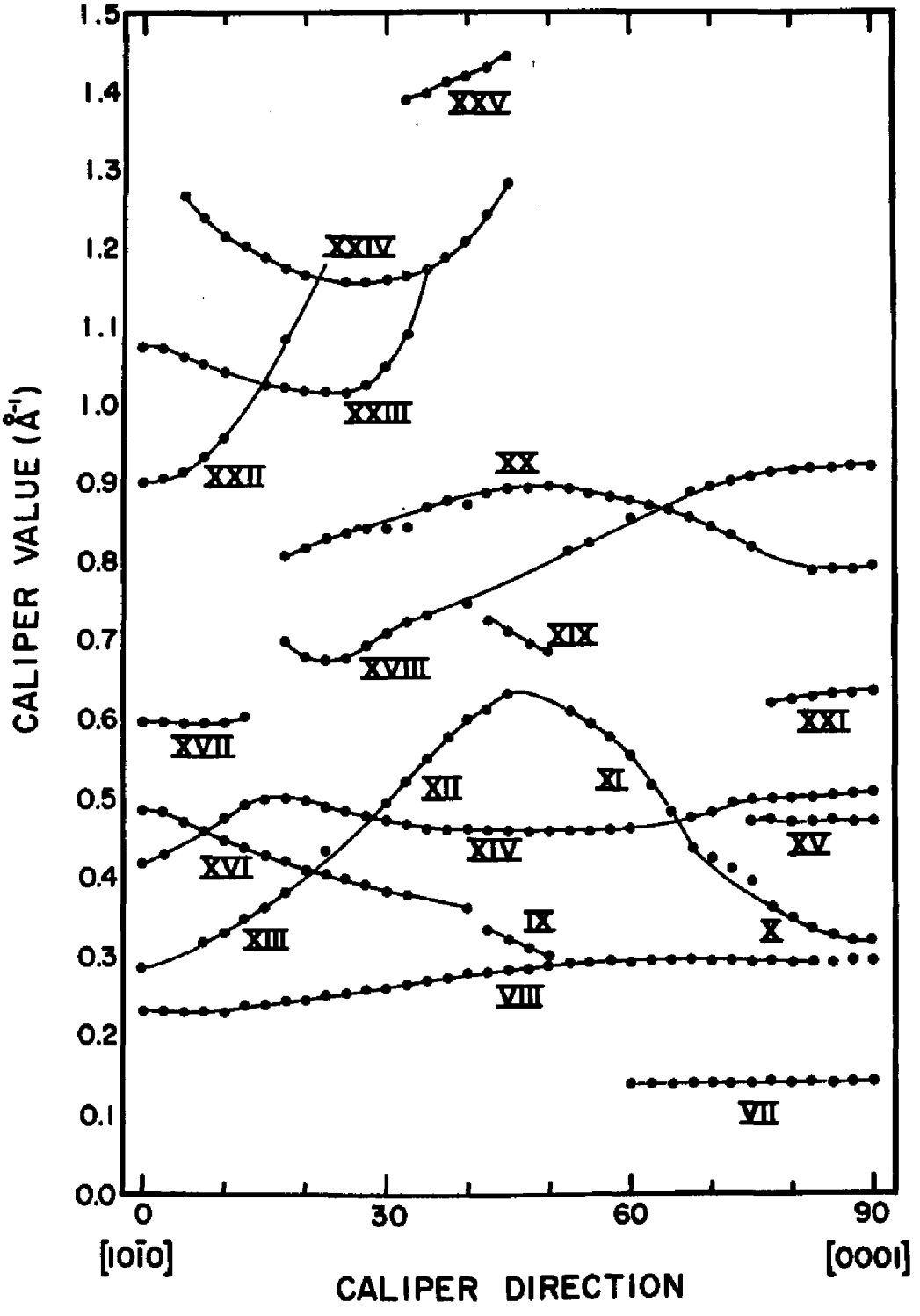

Fig. 17. Caliper vs. angle plot $\hat{n}\|[11\bar{2}0]$.

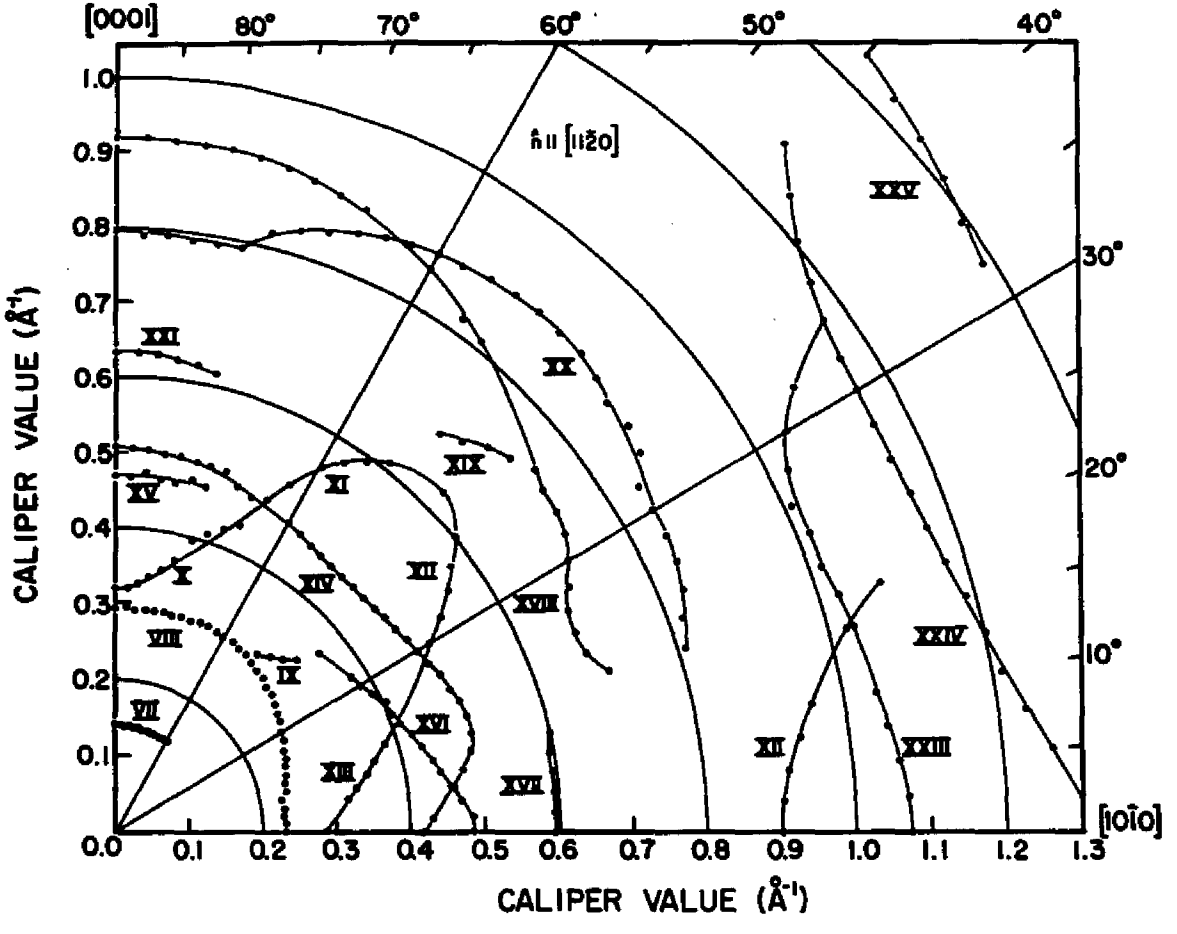

Fig. 18. Polar plot of calipers $\hat{n}\|[11\bar{2}0]$.

Table II

$\hat{n} \| [11\bar{2}0]$ d = 0.184 mm

Caliper Direction	Series VII	VIII	IX	X	XI	XII	XIII	XIV	XV	XVI	XVII	XVIII	XIX
$[10\bar{1}0]$		.231					.287	.419		.486	.597		
2.5		.231						.429		.484	.597		
5		.229						.456		.470	.595		
7.5		.231					.320	.456		.461	.595		
10		.229					.329	.475		.447	.595		
12.5		.238					.348	.491		.440	.602		
15		.238					.361	.498		.429			
17.5		.243					.380	.500		.422		.699	
20		.245					.410	.496		.408		.678	
22.5		.250					.433	.489		.405		.674	
25		.252						.484		.403		.676	
27.5		.257						.477		.392		.692	
30		.259				.493		.472		.382		.708	
32.5		.264				.521		.468		.378		.722	
35		.269				.549		.461				.729	
37.5		.273				.574		.459				.729	
40		.278				.600		.463		.361			
42.5		.278	.331			.611		.456					.724
45		.283	.320			.632		.456					.711
47.5		.283	.311					.455					.693
50		.287	.301					.458					.683

Table II (continued)

Caliper Direction	Series VII	VIII	IX	X	XI	XII	XIII	XIV	XV	XVI	XVII	XVIII	XIX
52.5		.290			.609			.458				.812	
55		.292			.593			.458				.822	
57.5		.294			.574			.463					
60	.137	.292			.553			.466				.856	
62.5	.139	.294			.514								
65	.137	.296			.482								
67.5	.139	.296			.435			.475				.889	
70	.139	.294			.424			.482				.893	
72.5	.139	.294			.410			.496				.900	
75	.139	.292			.396			.498	.468			.907	
77.5	.142	.294		.364				.498	.475			.912	
80	.139	.292		.350				.500	.468			.914	
82.5	.142	.292		.338				.500	.468			.916	
85	.139	.292		.327				.503	.475			.916	
87.5	.142	.294		.320				.505	.468			.919	
[0001]	.142	.294		.320				.507	.470			.919	

Table II (continued)

Caliper Direction	Series XX	XXI	XXII	XXIII	XIV	XV
[10$\bar{1}$0]			.900	1.074		
2.5			.905	1.071		
5			.912	1.060	1.266	
7.5			.933	1.051	1.238	
10			.956	1.041	1.212	
12.5					1.201	
15			1.023	1.030	1.187	
17.5	.808		1.083	1.023	1.173	
20	.815			1.016	1.164	
22.5	.831		1.178	1.016	1.164	
25	.836			1.007	1.155	
27.5	.838			1.025	1.157	
30	.840			1.048	1.157	
32.5	.840			1.088	1.162	1.390
35	.868				1.171	1.397
37.5	.877				1.187	1.414
40	.872				1.205	1.421
42.5	.884				1.242	1.430
45	.891				1.282	1.446
47.5	.889					
50	.896					
52.5	.886					
55	.884					
57.5	.879					
60	.879					
62.5	.870					
65	.866					
67.5	.856					
70	.842					
72.5	.833					
75	.817					
77.5	.789	.620				
80	.785	.623				
82.5	.787	.627				
85	.789	.632				
87.5	.789	.632				
[0001]	.794	.634				

C. Caliper Assignments

The calipers obtained from the $\hat{n}\|[11\bar{2}0]$ sample were easily assigned to various segments of the FS. The sizes of the resultant surfaces agree well with the dHvA measurements and the predictions of the band calculation. The caliper values obtained from the $\hat{n}\|[0001]$ sample could readily be assigned on the basis of their angular behavior but were consistently larger than the values predicted by any other measurements including the data from the other sample. A uniform reduction of these caliper values by 11.2% made them consistent with all previous and present results. Both the sample thickness and magnetic field calibration were checked but no cause could be found for this systematic error. A lack of sufficient starting material prevented the preparation of a second sample of this orientation.

The signal series I and VII have been assigned to the h_5 ellipsoids. When the magnetic field is along the $[10\bar{1}0]$ axis in each sample, signals arise from orbits about the waists of the ellipsoids. As the field is rotated from this direction these orbits extend further along the major axis of the ellipsoid and the signals become weaker as the band of participating electrons narrows. No signals were observed from these surfaces when the magnetic field was

more than 30° from the major axis of the ellipsoid. The signal series VII has been identified as a double field signal (two trajectories combine to span the sample), the primary signal occurring below the range of calipers obtained from this sample. The radii of $0.069\mathring{A}^{-1}$ along $[11\bar{2}0]$ and $0.036\mathring{A}^{-1}$ along [0001] agree well with the values of 0.063 and $0.037\mathring{A}^{-1}$ respectively obtained from the dHvA areas assuming elliptical orbits.

The signal series X through XIV and XVI from the $\hat{n}||[11\bar{2}0]$ sample have been assigned to the sixth band hole surface. The projections of this surface on the ΓALM plane and a plane rotated from ΓALM by 60° about the L-M line are shown in Figure 19. The extension of series XIV along the L-M line may be a little large due to overlap with the unidentified series XV. The existence of a closed orbit in the ALH plane giving rise to the caliper in the dimple along the A-L line indicates that this is a maximum dimension in this plane. This means that the intersection of h_6 with the ALH plane is ellipsoidal with no dimple at the ends. This surface is degenerate with h_5 on the A-L line and yields a caliper of $0.419\mathring{A}^{-1}$ which can be compared with the dHvA value of $0.438\mathring{A}^{-1}$ for the length of the ellipsoid.

The signals of series XVI with $\vec{H}$ parallel to [0001] arise from orbits of maximum diameter centered on the L-M line passing over the projections of h_6 in the ΓALM plane.

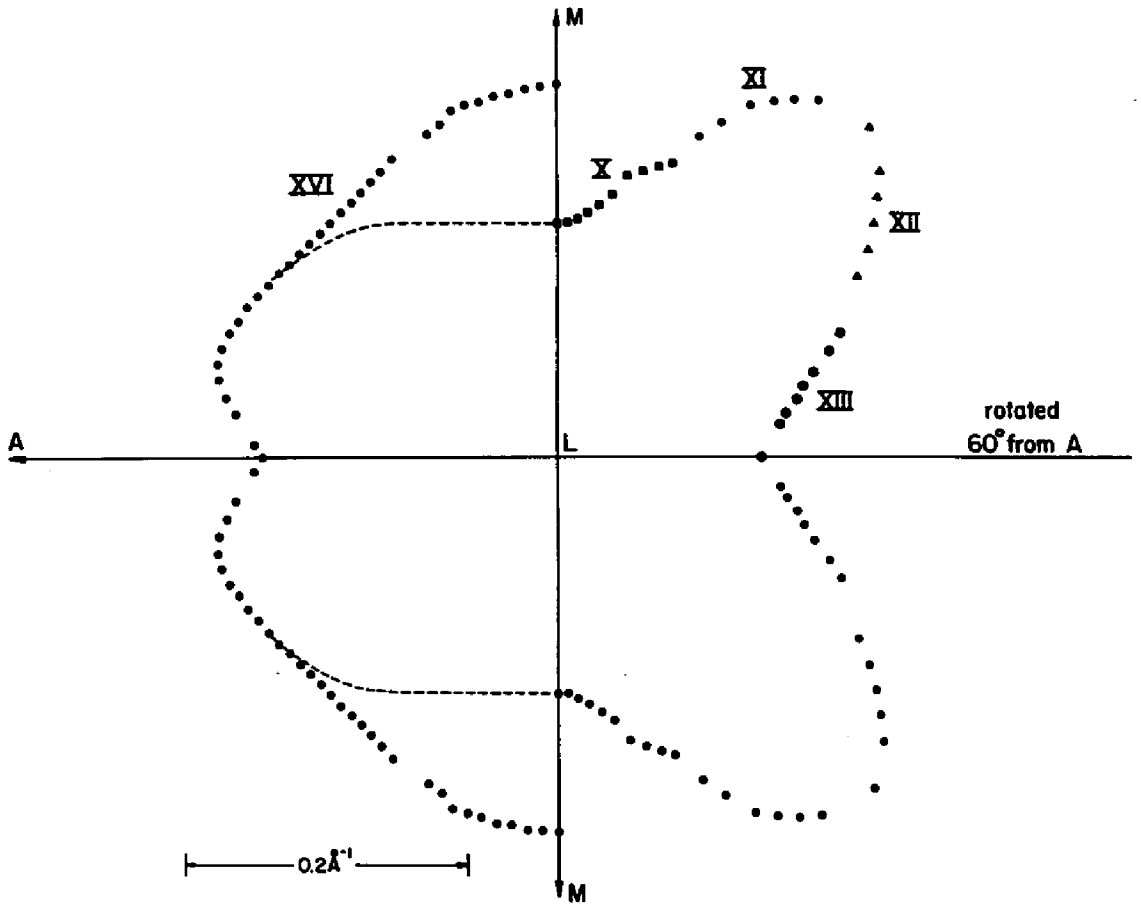

Fig. 19. Projections of the sixth band hole surface on various symmetry planes.

As $\bar{H}$ is rotated away from [0001], the signals of this series arise from orbits of minimal diameter with one edge passing through the A-L degeneracy point. Part of an orbit of minimal area in the ΓALM plane passing between the lobes of h_6 has been approximated by a dashed line in Figure 19. The area of this orbit has been calculated to be $0.135\mathring{A}^{-2}$ in good agreement with either of the values of 0.129 and $0.136\mathring{A}^{-2}$ determined by dHvA and theory. The signal series III obtained from the $\hat{n}\|[0001]$ sample gives an isotropic caliper (after reduction) of $0.461\mathring{A}^{-1}$ in excellent agreement with the other data for the radial extension of h_6 in all directions from the L-M line. This signal is actually a composite of three signals from the three different orientations of h_6 at the equivalent L points as shown in Figure 12. The strength and the uniformity of the line shape of this signal for all orientations of $\bar{H}$ in the basal plane show that although the maximum radial extensions occur at different heights above the ALH plane their lengths are the same. A three dimensional drawing of this surface appears in Figure 20. As can be seen from this figure this surface differs significantly from the dumbbell first proposed by Joseph and Thorsen[2] and might more correctly be described as a vertebra.

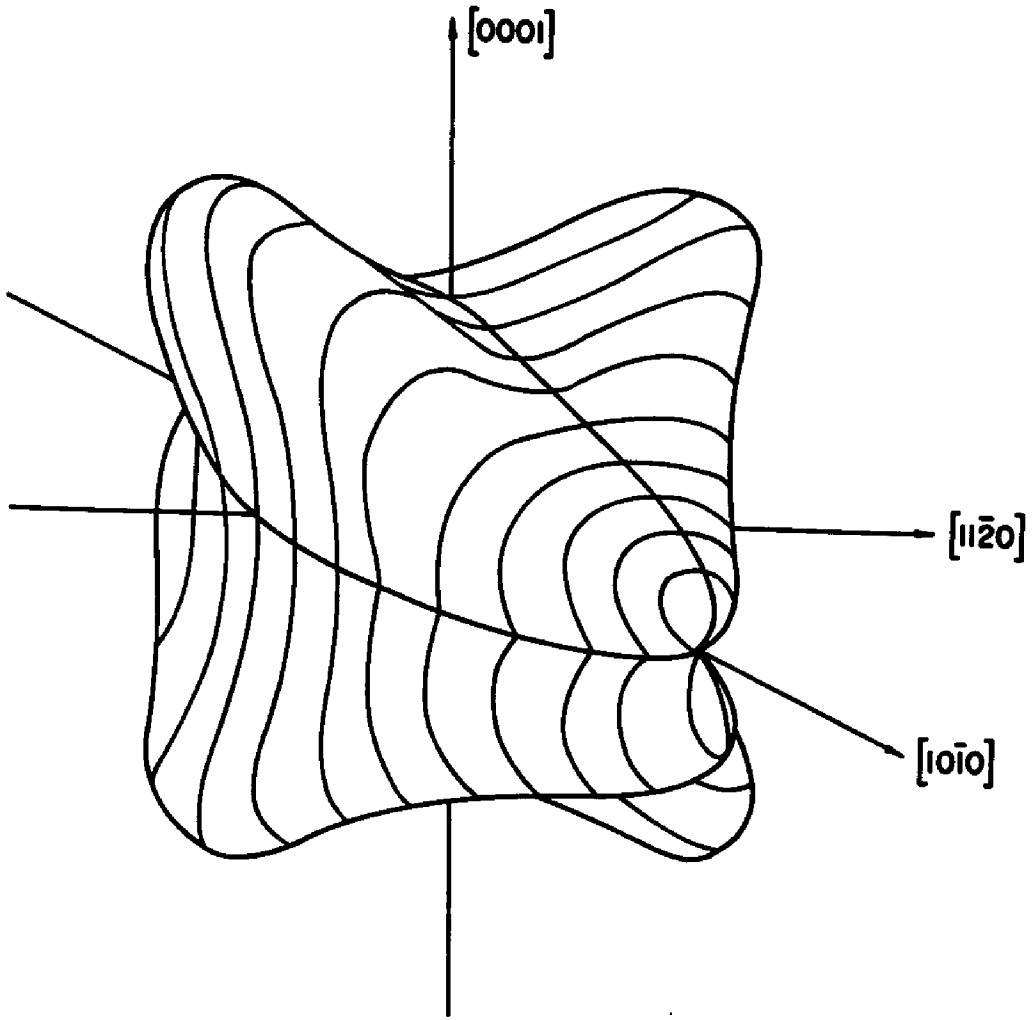

Fig. 20. Three dimensional drawing of the sixth band hole surface.

The signals of series V, VI, XVII, XVIII, and XX have been assigned to orbits about the seventh band hole surface. This surface can be considered as a construction of two simple surfaces. First an elliptical lens lies in the ALH plane. This shape is intersected by an elongated spheroid such that the long axis of the spheroid and the minor axis of the elliptical lens coincide along the L-H line ($[11\bar{2}0]$ direction). The projections of this surface on the ΓALM plane, a plane rotated from ΓALM by 60° about the L-M line, and the ALH plane are shown in Figure 21. The data indicate that this piece of surface is cleft top and bottom at the intersection with the ΓALM plane. When $\bar{H}$ is parallel to $[10\bar{1}0]$, the orbit giving rise to the signal of series XVIII lies in the LMKH plane. The caliper corresponds to the maximum extent of this orbit in the [0001] direction. This maximum occurs on either side of the cleft. The orbit giving rise to the series XX signal for this field orientation lies in a plane rotated 60° about the L-M line from the LMHK plane. This orbit passes through the cleft at a 30° angle without extending further in the [0001] direction and should give a good indication of the intersection of h_7 with the L-M line.

The signal series XVII has been assigned to orbits about the spheroidal part of h_7 above the plane of the lens when the field is near [0001]. These orbits do not seem

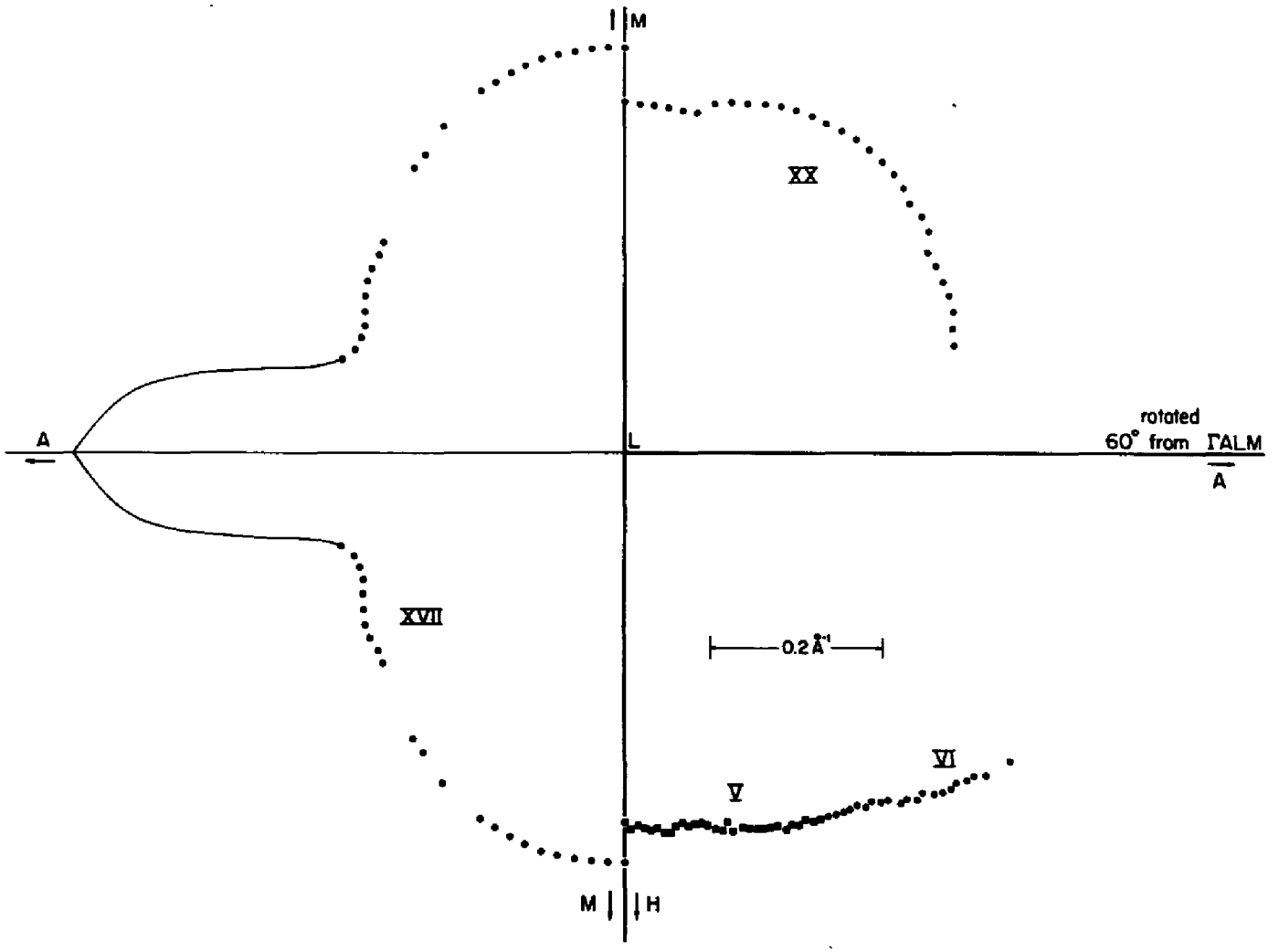

Fig. 21. Projections of the seventh band hole surface on various symmetry planes.

to be even local extrema but give rise to signals because of the abrupt change in the number of electrons participating in the transport of the r.f. electric field when the trajectories from these orbits span the sample. The extent of the lens portion of this surface has been approximated in Figure 21 from the intersection of the eighth band cylinder with which the lens is degenerate along the A-L line. From the e_8 calipers (to be presented shortly) this intersection is determined to lie $0.665\mathring{A}^{-1}$ from L. The angle of the intersection of e_8 with the A-L line is continued through the degeneracy point and the rest of the line is drawn to match to the calipers of series XVIII. The area of the resulting projection on the ΓALM plane is found to be $0.592\mathring{A}^{-2}$. This is about 10% smaller than the prediction of the band calculation ($0.648\mathring{A}^{-2}$) and would be smaller yet if the dimensions of the cleft could be properly taken into account. The calipers of series V and VI obtained from the $\hat{n}||[0001]$ sample have been assigned to the inersection of the lens of h_7 with the ALH plane as shown in the bottom right quadrant of Figure 21.

The projection of the eighth band cylinder on the ΓALM plane is shown in Figure 22. This figure has been constructed from the caliper series XXII through XXV. The series XXIII and XXIV arise from orbits centered at Γ and A respectively. Agreement between these sets of calipers

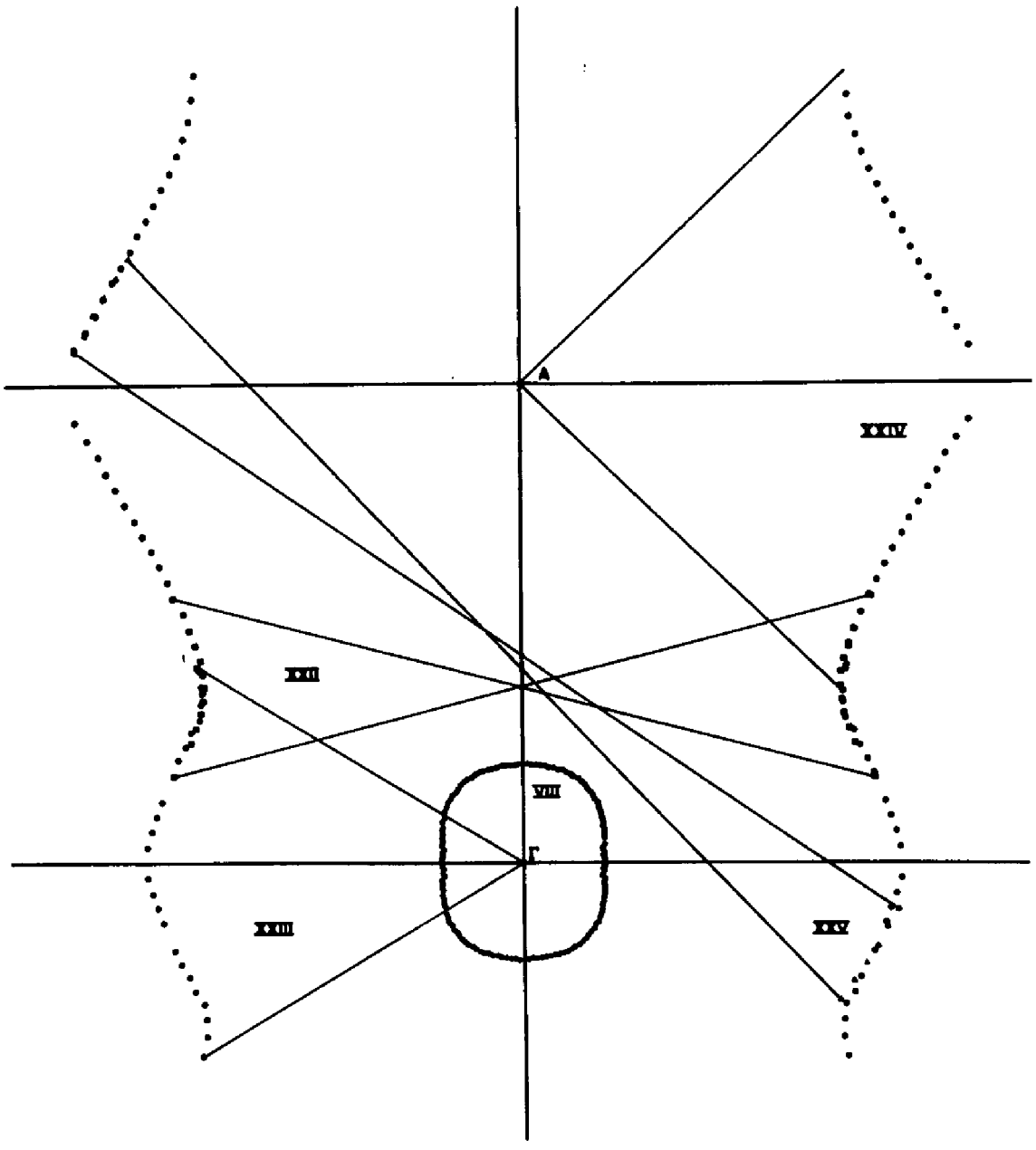

Fig. 22. Projections of the eighth band electron surface on the ΓALM plane.

on the position and diameter of the cylinder waist is very dependent on the determination of the caliper position on the signal and the sample thickness. The excellent agreement shown in the figure between these series and with the series XXII arising from minimal diameter orbits about the waist indicates that these determinations have been properly made.

The signal series IV obtained from the $\hat{n}\|[0001]$ sample has been assigned to the open orbits on the cylinder which caused the reduction in signal strength as a function of field orientation discussed earlier. The reduced caliper values from these signals vary smoothly from $0.598\mathring{A}^{-1}$ along $[11\bar{2}0]$ to $0.622\mathring{A}^{-1}$ along $[10\bar{1}0]$. This second caliper is much larger than can be expected for such an orbit in the ΓALM plane on the e_8 surface as predicted by the band calculation. An indentation in the cylinder parallel to the $[10\bar{1}0]$ direction between Γ and A might explain this caliper. If such an indentation did exist then the calipers from the A centered orbits of series XXIV and possibly the waist orbits of series XXII might be indicating the projection on the ΓALM plane of the intersection of the cylinder with the ΓAHK plane. A knowledge of the shape of the intersection of e_8 with the ΓAHK plane which might be obtained from an $\hat{n}\|[10\bar{1}0]$ sample would be most helpful in the further development of such a model.

The piece of surface centered at Γ in Figure 22 is a void in the eighth band surface. This void occurs where the eighth band rises above the Fermi energy near Γ. The recent dHvA results of Holroyd, Fawcett, and Perz[18] have demonstrated the existence of a closed piece of FS with a uniform area of 0.063Å^{-2} for all field orientations in the basal plane and 0.047Å^{-2} with $\vec{H}$ along [0001]. A harmonic of the signal from this piece was also observed for all field orientations. They assigned these areas to orbits about individual balls of the ninth band surface. This assignment was apparently influenced by the earlier assignment of partial series of these signals seen by Thorsen, Joseph, and Valby[3] to a ninth band torus. No dHvA data has been previously assigned to the eighth zone void.

Mattheiss[4] shows that an increase in the choice of the Fermi level from 0.825 to 0.830 Ry causes the topology of the ninth band to change from a set of distinct balls to a connected torus. For both of these levels the void in the eighth band surface still exists at Γ though it is slightly smaller at the higher energy. In both cases the intersection of the ninth band piece with the basal plane is far from circular as would be expected from symmetry considerations from its position in the zone. If, on the other hand, the Fermi level is reduced by 0.005 Ry, the ninth band piece disappears entirely and the eighth band void grows slightly. This situation yields a more

consistent analysis of both these recent dHvA measurements and the present data.

The resulting topology of the hole in the eighth band Fermi surface is that shown at Γ in Figure 22. Though the area is nearly 30% greater than that predicted by the theory the shape is very similar. The calipers of series VIII have been used to construct this figure. The calipers of series II with an isotropic value of $0.246\mathring{A}^{-1}$ (after reduction) from the basal plane data have also been assigned to this surface.

The results of the present measurements have met the expectations of the introduction. Several details of the shapes of various segments of the FS of rhenium, particularly the sixth band piece, have been determined. These measurements also indicate that the shape of the eighth band cylinder may be more complicated than previously thought. The areas of extremal orbits over these pieces agree with and show the shapes to be consistent with previous dHvA measurements. It has been determined from these measurements and the recent dHvA measurements of Holroyd, et al., that no evidence presently exists to indicate the presence of a ninth band electron surface in rhenium. All previous measurements which have been attributed to such a surface can be explained in terms of the eighth band void at Γ the topology of which is much less sensitive to the Fermi level.

It is indeed regrettable that the data obtained from the $\hat{n}||[0001]$ sample have had to be scaled down. The internal and external consistency so obtained does however seem to justify this action. Data from an $\hat{n}||[10\bar{1}0]$ sample would be helpful on two counts. Signals from such a sample arising from orbits about h_7 could give more information on the nature of the cleft in this surface. Whether such signals could be observed from orbits passing through the A-L degeneracy is not known. Such a sample could also provide information on the intersection of the e_8 cylinder with the ΓAHK plane which would be very useful in determining the actual shape of this piece of FS.

CHAPTER V

TEMPERATURE DEPENDENCE MEASUREMENTS

For many years the low temperature electrical resistivity of transition metals has been found to obey a T^2 law. While electron-electron (e-e) scattering should give rise to a T^2 dependence of resistance, simple theories of this scattering process do not readily lend themselves to an evaluation of the magnitude of the e-e scattering frequency. Other mechanisms involving transport processes have been proposed to explain the observed T^2 dependent results.[19] A T^2 dependence has also been observed in the amplitude of the RFSE signals in W and Mo.[20] In the RFSE the temperature dependence of the amplitude of the signal arises from an isolated group, or orbit, of electrons on a particular sheet of the Fermi surface (FS) and is not affected by complicated transport effects.

RFSE measurements were performed on a sample 0.231 mm thick ($R_{300}/R_{4.2} \simeq 20{,}000$) and having $\hat{n} \| [11\bar{2}0]$. Temperature-dependent data were taken on the signal arising from an extremal orbit centered around the A point in the Brillouin zone of the h.c.p. structure on the eighth-band electron sheet of the FS when the magnetic field was directed 22° from [0001] toward $[10\bar{1}0]$.[21] This was the strongest signal observed at any orientation of $\vec{H}$ in this

sample and for this sample thickness it occurs at fields (400 G) above the superconducting critical field for all temperatures investigated. Since these results were obtained from the thickest sample in which the RFSE could be observed, the single pass limit formula (Eq. 6) is appropriate.[22] The temperature dependence of $\bar{\nu}$ is determined by a measurement of the temperature dependence of the amplitude of the RFSE signal, A. A plot of the ℓn of the signal amplitude vs T^2 is shown in Figure 23. Each point on this plot represents four measurements of the amplitudes at each temperature. The error bars represent one standard deviation above and below the mean amplitude.

A least squares fitting routine was used to determine the best coefficients s and x to fit the data to

$$\ell n\ A/A_o = -sT^x. \qquad (11)$$

For all the data as shown these values were: s = 0.0192 and x = 2.56. As the highest temperature points were sequentially removed from the data set the value of x steadily decreased. This decrease stopped after all the points from temperatures greater than 5K ($T^2 = 25K^2$) had been removed from the set. All the data below this point fit best with s = 0.0492 and x = 2.00. This line is shown on the plot of Figure 23. This data can thus be fit to

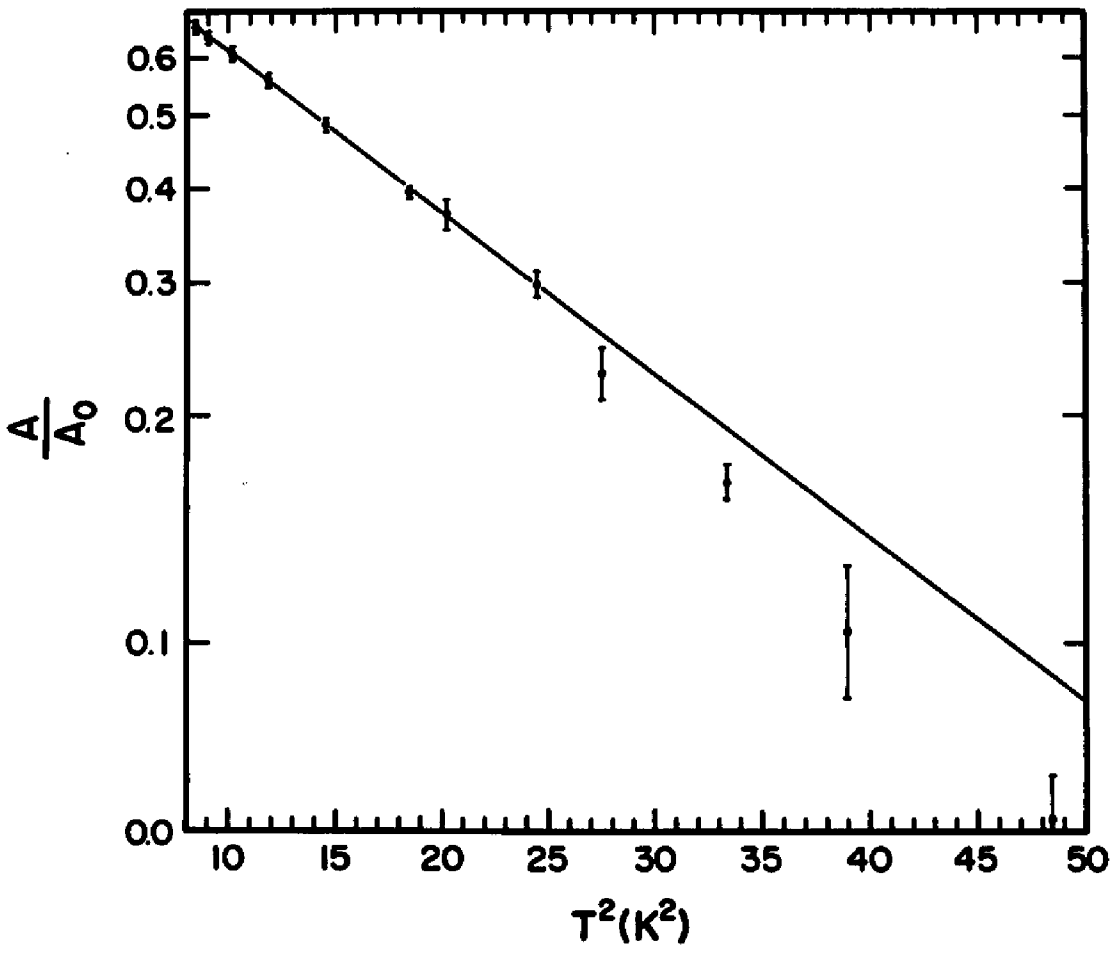

Fig. 23. Temperature dependence of the amplitude of the RFSE signal obtained with $\bar{H}$ 22° from [0001] in the $\hat{n} \| [11\bar{2}0]$ sample.

$$\ell n\ A/A_o = -\frac{\pi}{\Omega}\bar{\nu} = -\alpha T^2 \qquad (12)$$

below 5 K.

In order to determine the value of $\bar{\nu}/T^2$ from this data, the cyclotron frequency for this orbit at the value of the applied field of the RFSE signal must be known. The effective mass for this orbit was determined from Azbel-Kaner geometry cyclotron resonance measurements (see Appendix) to be 1.6 m_o. Writing the scattering frequency for this orbit as $\bar{\nu}(T) = aT^2$ and incorporating the measured effective mass into Eq. (12) gives the value $a = 7.1 \times 10^{-7}/\text{sec-K}^2$.

The result of this experiment and the results of RFSE measurements on tungsten and molybdenum as well as resistance measurements on all three metals are shown in Table III. It can be seen that the correlation between the RFSE results a and the resistance results A_R (where $\rho = \rho_o + A_R T^2$) are good. The averaged values of a for tungsten are slightly less than for molybdenum and both are a factor of three to four less than for rhenium. The same holds true for the coefficient of the T^2 term of the resistance of these three metals. It is seen that for these three metals the T^2 dependence of the resistance is a reasonable indicator of an intrinsic property of the scattering cross section for conduction electrons.

The present results suggest that when a T^2 dependence of the resistivity of a metal is observed, the slope of

Table III

Coefficients of the Temperature-squared Dependent Scattering Frequencies and Resistances for W, Mo, and Re

Metal	$a \times 10^7$ $(K^2\ sec)^{-1}$	$A_R \times 10^{11}$ $(\Omega cm/K^2)$
W	2.0[a]	.055[c]
Mo	2.4[a]	0.126[d]
Re	7.1[b]	0.45[e]

[a]From Ref. 20. These are average values for the eight orbits examined with unit weightings for each.

[b]Present results.

[c]E. L. Stone, M. D. Ewbank, J. Bass, and W. P. Pratt, Jr., Phys. Lett. 59A, 168 (1976).

[d]T. L. Ruthruff, C. G. Grenier, and R. G. Goodrich, Phys. Rev. B 17 (1978).

[e]J. T. Shriempf, J. Phys. Chem. Solids 28, 2581 (1967).

this dependence is indicative of the strength of the e-e scattering. The coefficients of the T^2 dependence of the low temperature resistivities of the transition metals: V, Fe, Co, Zr, Ni, Nb, Ru, Pd, W, Re, Os, Ir, and Pt have been reported in the literature. These coefficients are shown in Table IV. An important feature of this table is that a T^2 dependence has been observed in all transition metals which have been subjected to careful low temperature resistance measurements. Measurements of the RFSE have not been made on any of the transition metals other than W, Mo, and Re. Outside of this group of metallic elements e-e scattering has not been observed either in resistance or RFSE measurements in the temperature range of 1-4 K. The reported T^2 dependence of the resistance of both bismuth and antimony has now been attributed to a very low effective Debye temperature for electron-phonon scattering.[23,24] In particular when the d bands are exactly filled (the noble metals) both the RFSE amplitude and the resistance are dominated by electron-phonon scattering in this temperature range.

Several mechanisms have been suggested to account for the enhanced e-e scattering in transition metals. They are: the complicated Fermi surface topology of transition metals, the wide variation in carrier effective masses in transition metals, and the high electron density of states

Table IV

Partial Periodic Table of Transition Metals Giving the Value of A_R in $\rho = \rho_o + A_R T^2$ Between 1 and 4 K in Units of $10^{-11}\Omega$-cm/K^2

(S - superconducting in measurement range)

3d	Sc	Ti	V	Cr	Mn	Fe	Co	Ni	Cu
			S			3.1	.98	3.4 .95[a]	0
4d	Y	Zr	Nb	Mo	Tc	Ru	Rh	Pd	Ag
			.23[a] S	0.126	S	.27		3.1	0
5d	La	Hf	Ta	W	Re	Os	Ir	Pt	Au
	S		S	0.1	0.45	0.2		1.4	0

[a]Corrected for magnetoresistance.

Fe - J. G. Beitchman, C. W. Trussel, R. V. Coleman, Phys. Rev. Lett. 25, 1291 (1970). Note this value is not corrected for magnetoresistance.

Co - D. Radhakrishma, Phys. Stat. Solidi 11, 111 (1965). Note this value is not corrected for magnetoresistance.

Ni - G. K. White and R. J. Tanish, Phys. Rev. Lett. 19, 165 (1967).

[a]F. C. Schwerer and J. Silcox, Phys. Rev. Lett. 20, 101 (1968).

Nb - [a]G. W. Webb, Phys. Rev. 181, 1127 (1969).

Mo - T. L. Ruthruff, C. G. Grenier, and R. G. Goodrich, Phys. Rev. B 17, (1978).

Ru - J. T. Schriempf and W. M. Macinnes, Phys. Lett A 33, 511 (1970).

Pd - J. T. Schriempf, Phys. Rev. Lett. 20, 1034 (1968).

W - D. K. Wagner, J. C. Garland, and R. Bowers, Phys. Rev. B 3, 3141 (1971).

Re - J. T. Schriempf, Solid State Comm. 6, 813 (1968).

Os - J. T. Schriempf, Solid State Comm. 6, 813 (1968).

Ir - N. V. Valkenshtui, et al., Phys. Met. and Metall. 31, 212 (1971).

Pt - C. Uher, C. W. Lee, and J. Bass, Phys. Lett. 61A, 344 (1977).

combined with high Debye temperatures for this group of elements.

Ziman[25] shows that in a metal the Normal e-e scattering processes between electrons of like mass will not affect the resistivity. Scattering processes between electrons of like mass contribute to the resistivity only when Umklapp processes are involved. Topologically complicated, multiply-connected Fermi surfaces make such U processes much more favorable. The Fermi surfaces of the transition metals usually satisfy this condition and this could lead to an enhancement in the e-e scattering rate. However, the Fermi surfaces of several non-transition metals such as the poly-valent hexagonal close-packed metals Mg, Zn, and Cd also penetrate the zone boundaries and are fully as complicated as those of the transition metals. Yet the resistivity and RFSE of each of these metals is dominated entirely by electron-phonon scattering in the temperature range above 1 K.

Normal electron-electron scattering processes can contribute to the resistivity if the electrons involved have significantly different masses. The magnitude of this effect is proportional to the magnitude of the variation of the masses in a particular metal. The effective masses of the charge carriers in Mo and W range from 0.40 to 2.50 and 0.27 to 1.83 respectively on the orbits studied by Boiko, et al. This is a variation of slightly over six in

both cases. The effective masses of the carriers in In, Al, Tl, Cd, Zn, and Mg vary by an order of magnitude or more in each case.[26] In each of these non-transition metals the low temperature resistivity is dominated by electron-phonon scattering.

Boiko, et al., have suggested that the high electron density of states as measured by the electronic specific heat and the high Debye temperatures of the transition metals might yield information about the enhanced e-e scattering ratio. The relatively high electron concentrations and low phonon concentrations indicated by these parameters at low temperatures might provide for a greater predominance of e-e scattering over e-p scattering. Copper exhibits relatively high values for these quantities and yet is known to have a temperature-dependent resistivity dominated by e-p scattering down to 1 K. The values for Al are even higher than for W but recent results[27] have shown that the low temperature resistivity of this metal is also dominated by e-p scattering.

These considerations show that while large effective mass differences, large densities of states and complicated Fermi surfaces may be necessary for the observation of e-e scattering above 1 K, they are not by themselves or in combination sufficient to explain the observed T^2 dependence of resistivity above 1 K. Only when electron states near

the Fermi level which are strongly hybridized by d-states (3-d, 4-d and 5-d transition metals) is the T^2 dependence observed. The matrix element which determines the scattering probability for this effect must be strongly dependent on the orbital angular momentum of the electrons involved. Variations between transition metals may be explained by structural, density of states at the Fermi level, or Fermi surface complications, but the overall magnitude of the effect must be due to an increased size of the scattering matrix element caused by the influence of d-bands.

REFERENCES

1. A. C. Thorsen and T. G. Berlincourt, Phys. Rev. Lett. 7, 244 (1961).
2. A. S. Joseph and A. C. Thorsen, Phys. Rev. 133, A1546 (1964).
3. A. C. Thorsen, A. S. Joseph, and L. E. Valby, Phys. Rev. 150, 523 (1966).
4. L. F. Mattheiss, Phys. Rev. 151, 450 (1966).
5. W. A. Reed, E. Fawcett, and R. F. Soden, Phys. Rev. 139, A1557 (1965).
6. C. K. Jones and J. A. Rayne, Phys. Rev. 139, A1876 (1965).
7. L. R. Testardi and R. R. Soden, Phys. Rev. 158, 581 (1967).
8. D. K. Wagner and R. Cockran, J. Low Temp. Phys. 18, 549 (1975).
9. V. F. Gantmakher, Rep. Prog. Phys. 37, 317 (1974).
10. R. R. Soden, G. F. Brennert, and E. Buehler, J. Electrochem. Soc. 112, 77 (1965).
11. D. A. Boudreaux and R. G. Goodrich, Phys. Rev. B 3, 3086 (1971).
12. O. L. Steenhaut, Ph.D. Dissertation, Louisiana State University (1970).
13. W. D. Knight, Rev. Sci. Instr. 32, 95 (1961).

14. A. J. Slavin, Cryogenics 12, 121 (1972).

15. M. R. Holman, 3rd year undergraduate report, University of Bristol, England (1973).

16. E. A. Faulkner and A. Holman, J. Sci. Instr. 44, 391 (1967).

17. G. E. Juras, Phys. Rev. 187, 784 (1969).

18. F. W. Holroyd, E. Fawcett, and J. M. Perz, Proc. of Int. Conf. on Transition Metals, Toronto, August 1977.

19. D. K. Wagner, Phys. Rev. B 5, 336 (1972).

20. V. V. Boiko, V. F. Gantmakher, and V. A. Gasparov, Sov. Phys.-JETP 33, 584 (1971).

21. R. G. Goodrich and T. L. Ruthruff, Proc. of Int. Conf. on Transition Metals, Toronto, August 1977.

22. P. B. Johnson, J. C. Kimball, and R. G. Goodrich, Phys. Rev. B 14, 3282 (1976).

23. C. Uher and W. P. Pratt, Jr., Phys. Rev. Lett. 39, 491 (1977).

24. C. L. Tsai and C. G. Grenier, to be published in Phys. Rev. B.

25. J. M. Ziman, Electrons and Phonons (Clarendon Press, Oxford, 1960), p. 412.

26. For a review of Fermi surface properties see P. B. Visscher and L. M. Falicov, Phys. Stat. Sol (b) 54, 9 (1972).

27. V. A. Gasparov and N. H. Harutunian, Solid State Comm. 19, 189 (1976).

Other references used but not explicitly cited:

N. W. Ashcroft and N. D. Mermin, Solid State Physics, Holt, Rinehart, and Winston, New York, 1976.

R. G. Chambers, Phys. Kondens. Materie 9, 171 (1969).

V. F. Gantmakher, Prog. Low Temp. Phys. 5, 181 (North-Holland, Amsterdam, 1967).

APPENDIX

EFFECTIVE MASS MEASUREMENT

In order to determine the electron scattering frequency from the temperature dependence of the RFSE signal amplitude, the cyclotron frequency, Ω, of the electrons about the signal trajectory must be known. As can be seen from Eq. (3) this frequency depends not only on the value of the magnetic field at which the signal occurs but also on the effective mass of the electrons on this orbit, m^*. To determine this mass Azbel-Kaner geometry cyclotron resonance measurements were made.

An end plate was made to hold the $\hat{n}||[11\bar{2}0]$ sample in position as part of the bottom surface of a TE_{103}, 35 GHz microwave resonant cavity. This cavity was attached to a microwave spectrometer and the strength of the reflected microwaves was monitored as a function of klystron tuning for a dip corresponding to absorption at the resonant frequency of the cavity. Several dips arising from impedance mismatches in the spectrometer were also detected but that from the cavity could be identified by loosening the bottom plate and observing the frequency shift as it was moved slightly. Use of the absorption wavemeter in the system showed this frequency to be 35.42 GHz. The size of the small hole in the silver disc between the waveguide and the cavity was increased by gradual increments to

improve the coupling until only a very small portion of the microwave energy was reflected at the cavity resonant frequency.

A speck of 2,2-Diphenyl-1-picrylhydrazyl (DPPH) was glued to the bottom plate of the cavity. Observation for the very strong EPR signal from the DPPH allowed identification of the cavity resonance from others of the system when the cavity had been cooled in liquid helium. The cavity, at the end of a section of silver plated thin wall stainless waveguide, was placed in the conventional dewar system between the poles of the Varian magnet. Five inch diameter pole faces had been fit to the magnet to allow magnet fields of 15 kG to be attained in the vicinity of the sample.

The cavity resonance was monitored carefully as the system was precooled to 77K. Thermal contraction of the cavity caused the resonant frequency to increase during the cooldown. Up to this point the sweep unit of the klystron power supply had been used to continuously sweep the reflector voltage through one of the klystron oscillation modes. The klystron was mechanically tuned to center this mode on the resonant frequency of the cavity. With introduction of liquid helium to the system the resonant frequency shifted much too rapidly to be followed.

The magnet was rotated so that the field was directed through the narrow dimension of (parallel to the electric field in) the waveguide. In this optimum configuration each dip of the microwave reflectance spectrum was examined for the EPR signal in the range of 12 to 13 kG. The cavity resonance was finally found at 34.48 GHz. The dielectric properties of the liquid helium in the cavity made its effective length longer and had more than offset the effects of thermal contraction.

The sweep was removed from the reflector and its voltage was adjusted to center on the resonance dip. A klystron stabilizer was engaged to control the reflector voltage and keep the klystron tuned to the frequency of the cavity even if it should drift slightly due to a signal resonance. The magnet was rotated 90° so that the magnetic field would be perpendicular to the microwave electric field as in RFSE measurements. Electrons traveling on trajectories normal to the magnetic field direction would thus travel parallel to the electric field and interact with it at the sample surface. The sample had been placed in its holder so that the magnetic field would be directed 22° away from the [0001] axis when oriented this way. This was the direction in which the temperature dependence measurements had been made.

The sample absorbs energy from the microwave electric field when the electron cyclotron frequency is an integral divisor of the microwave frequency (ω)

$$\Omega = \frac{eH}{m^*c} = \frac{\omega}{n}. \tag{12}$$

As the magnetic field is swept, absorption signals are observed when

$$H = \frac{m^*c}{e}\frac{\omega}{n} = \frac{H_R}{n}. \tag{13}$$

Several series of weak resonances were observed as the magnetic field was oriented over a 20° range about the previously selected direction. The strongest series was seen for n = 2,3,4,5, and 6 and H_R = 19.55 kG (note: this primary signal could not be seen because of the 15 kG limit of the magnet). From this series the effective mass could be calculated from

$$m^* = \frac{H_R e}{\omega c} \tag{14}$$

to be $m^* = 1.6\ m_o$. The cyclotron frequency at 400 G for this orbit was then calculated to be 4.49×10^9 rad/sec and this value was used to determine the electron-electron scattering frequency from the temperature dependence of the RFSE signal amplitude.

VITA

Terrence L. Ruthruff was born in Oregon City, Oregon, on October 7, 1949. His secondary education was completed at Leuzinger High School in Lawndale, California, and in October 1967 he enrolled in the University of California at Los Angeles where he received a Bachelor of Science degree in Physics Cum Laude in 1971. The following fall he enrolled for graduate study in physics at Louisiana State University where he received his Master of Science degree in Physics in May 1973. He is presently a candidate for the degree of Doctor of Philosophy.

EXAMINATION AND THESIS REPORT

Candidate: Terrence L. Ruthruff

Major Field: Physics

Title of Thesis: Radio Frequency Size Effect Measurements on the Fermi Surface of Rhenium

Approved:

Major Professor and Chairman

Dean of the Graduate School

EXAMINING COMMITTEE:

Date of Examination:

February 27, 1978